EFFECTS OF CLOGGING, ARGON INJECTION AND CONTINUOUS CASTING CONDITIONS ON FLOW AND AIR ASPIRATION IN SUBMERGED ENTRY NOZZLES

Hua Bai and Brian G. Thomas

Hua Bai, Senior research engineer, is with the Dow Chemical Company, 2301 N. Brazosport Blvd., Freeport, TX 77541, and Brian G. Thomas, Professor, is with the Department of Mechanical and Industrial Engineering, University of Illinois at Urbana-Champaign, 1206 W. Green Street, Urbana, IL 61801

ABSTRACT

The inter-related effects of nozzle clogging, argon injection, tundish bath depth, slide gate opening position and nozzle bore diameter on the steel flow rate and pressure in continuous-casting slide-gate nozzles are quantified using computational models of three-dimensional multiphase turbulent flow. The results are validated with measurements on operating steel continuous slab-casting machines, and are presented for practical conditions with the aid of an inverse model. Predictions show that initial clogging may enhance the steel flow rate due to a potential streamlining effect before it becomes great enough to restrict the flow channel. The clogging condition can be detected by comparing the measured steel flow rate to the expected flow rate for those conditions, based on the predictions of the inverse model presented here. Increasing argon injection may help to reduce air aspiration by increasing the minimum pressure, which is found just below the slide gate. More argon is needed to avoid a partial vacuum effect at intermediate casting speeds and in deeper tundishes. Argon flow should be reduced during shallow tundish and low casting speed conditions (such as encountered during a ladle transition)

in order to avoid detrimental effects on flow pattern. Argon should also be reduced at high casting speed, when the slide gate is open wider and the potential for air aspiration is less. The optimal argon flow rate depends on the casting speed, tundish level, and nozzle bore diameter and is quantified in this work for a typical nozzle and range of bore diameters and operating conditions.

KEY WORDS: clogging, air aspiration, continuous casting, tundish-mold, nozzle, multiphase turbulent flow, numerical models, computational fluid dynamics, submerged entry nozzle, slide gate, argon

I. INTRODUCTION

Nozzle clogging is one of the most disruptive phenomena in the operation of the tundish-mold system in continuous casting of steel and has received much study [1-3]. Nozzle clogs are suspected to adversely affect product quality in several ways. First the clog may change the flow pattern in the mold, which is usually carefully designed based on the assumption of no clogging. Mold level variations and unstable flow in the mold are more severe with clogging [4]. Secondly, the internal quality of the final product is seriously compromised whenever chunks of a nozzle clog break off and enter the flow stream. Clogs trapped in the solidifying steel form inclusion defects that drastically lower strength and toughness [1]. Even if it is not entrapped in the solidified steel, a large clog can be detrimental if it suddenly floats into the slag layer. It may cause sudden level surges, which are well-known to cause surface quality problems. The alumina added from a clog can also disrupt the local slag composition and increase slag viscosity, which can make slag infiltration at the meniscus more difficult, and thereby lead to surface defects such as longitudinal cracks. Finally, as the buildup progresses, the slide gate opening must be

increased to maintain the desired flow rate. Once the slide-gate reaches its maximum position, production must stop and the nozzle must be replaced. Thus, its important to find and understand ways to both detect and prevent clogging.

Argon injection into the nozzle is widely employed to reduce nozzle clogging, even though its working mechanisms are still not fully understood [1]. In addition, the injected argon bubbles affect the flow pattern in the nozzle, and subsequently in the mold. Some bubbles may attach with small inclusions and become entrapped in the solidifying shell, resulting in "pencil pipe" and blister defects on the surface of the final product [5-7]. Other possible disadvantages of argon injection observed in operation include increased quality defects and nozzle slag line erosion due to the increased meniscus fluctuation [8, 9], exposure of the steel surface and subsequent reoxidation [10], entrapment of the mold power [11], and emulsification of the flux layer, leading to flux-gas foams, which are easily entrained as inclusional defects [12]. Large gas injection flow rates might create a boiling action in the mold [13], which can greatly intensify those adverse effects. Thus, it is important to optimize argon injection to the minimum amount needed to achieve its benefits.

Air aspiration through cracks, joints or porous refractory into the nozzle leads to reoxidation, which is an important source of inclusions and cause of clogging [13, 14]. Air aspiration is more likely if the pressure inside the nozzle drops below atmospheric pressure, creating a partial vacuum. Mathematical modeling of the pressure profile along the nozzle has been reported for both liquid only [15] and liquid-gas systems [16, 17]. While regulating the liquid steel flow, the slide-gate creates a local flow restriction, which generates a large pressure drop [1]. This creates a low-pressure region just below the throttling plate, which often falls below 1 atm (0 gauge pressure). Measurements of the partial vacuum pressure generated by the throttling of the slide gate have been reported for water model experiments in both tundish nozzles [14] and

ladle shrouds [15]. These experimental studies show that the partial vacuum in the nozzle could be reduced by increasing the gas flow rate [14, 18] or pressurizing the nozzle [18]. The minimum pressure inside the nozzle is affected by argon injection, tundish bath depth, casting speed, gate opening and clogging. Predicting when a partial vacuum condition exists and choosing conditions to avoid it is one way to prevent this potential source of reoxidation products and the associated clogging and quality problems.

Flow through the tundish nozzle is gravity-driven by the difference between the liquid steel levels in the tundish and in the mold. Flow rate or casting speed depends upon the tundish bath depth, the position of the slide gate and other flow characteristics inside the nozzle. Both clogging and argon injection may greatly affect the flow pattern in the nozzle, and subsequently in the mold, by altering the flow rate, the flow symmetry, and flow transients, and thereby cause quality problems. Thus, there is incentive to understand quantitatively how they are related to the operation variables.

In practice, the operation variables are interrelated. Changing one variable usually causes corresponding changes in another variable. For example, a drop in tundish bath depth needs a corresponding increase in gate opening in order to maintain a constant casting speed. During a stable casting process, tundish bath depth and argon injection are usually kept constant, and gate opening is regulated to compensate for any unwanted effects, such as nozzle clogging, in order to maintain both a constant casting speed and steel level in the mold.

In this paper, a mathematical model is developed to relate argon injection, tundish bath depth, casting speed, and gate opening for practical slab casting conditions. The influence of nozzle clogging and nozzle bore size are also investigated. This model is derived from interpolation of the numerical simulation results of a three-dimensional model of the two-phase turbulent flow of liquid steel and argon bubbles in tundish nozzles. Model predictions are

compared with plant measurements. The model is then extended to predict the minimum pressure in the nozzle as a function of the same casting conditions. Finally, the model is applied to investigate operating conditions to avoid partial vacuum pressures, including the optimal flow rate of argon gas.

II. MODEL FORMULATION

A model to investigate the interrelated effects of casting variables on the minimum pressure in the nozzle is developed in five stages. First, a 3-D finite-volume model, which was developed and validated in previous work, is used to perform a parametric study. Then, the output pressure drops across the nozzle are converted to corresponding tundish bath depths and the results are curve fit with simple equations. Next, these equations are inverted to make the tundish bath depth an independent variable and to allow presentation of the results for arbitrary practical conditions. Finally, the predicted minimum pressure results are combined with the inverse model, so that they also can be presented for practical casting conditions.

A. 3-D Finite volume Model

A three-dimensional finite volume model was developed to study the time-averaged two-phase turbulent flow of molten steel and argon bubbles in slide-gate tundish nozzles using the multi-fluid Eulerian multiphase model [19]. For each 3-D simulation, the numerical model solves two sets of Navier Stokes equations, and equations for continuity and transport of K and ε. It calculates the gas and liquid velocity vector fields, the gas fraction, and the pressure everywhere within the domain of the entire nozzle (no symmetry).

The computational domain for simulating flow through a typical slide-gate nozzle is shown in Figure 1 with its boundary conditions. The top of the nozzle is attached to the tundish bottom and the outlet ports exit into the continuous casting mold. In this model, the chosen slide

gate opening position is incorporated into the computational domain during mesh generation. Inlet boundary conditions for the liquid steel and argon flow rates are set by fixing uniform normal velocity at the top of the nozzle and at the gas injection region of the upper tundish nozzle (UTN) respectively. Bubbly flow is assumed with the model, which means that the effects of large voids that might form below the gate are neglected. The model equations are solved with the CFX4.2 code [19] on a mesh containing 34,000 nodes. Each complete simulation requires about 2.5 hours to execute on one SGI Origin 2000 processor. Further details on the model are described elsewhere [16]. The accuracy of flow predictions near the port outlet has been verified both qualitatively by comparison with visual observations of water model experiments and quantitatively by comparison with velocity measurements using Particle Image Velocimetry [16].

B. Parametric Study with 3-D Computational Model

The 3-D computational model is employed here to simulate the turbulent flow of liquid steel with argon bubbles in a typical slide-gate nozzle, and to perform an extensive parametric study of relevant operating conditions including casting speed, gate opening, argon injection flow rate and nozzle bore diameter. Over 150 simulations are performed, based on the standard nozzle in Figure 1 with the standard geometry and conditions given in Table I. This nozzle is typical of a conventional slab casting operation. It has a 90° orientation slide-gate, so the right and left sides of the mold are nominally symmetrical. This orientation has the least bias flow between the two ports, so is widely adopted in practice. Figure 2 shows typical simulated velocity vectors and argon gas distribution.

The different conditions of the parametric study are listed in Table II. Casting speed V_C refers to a typical size of the continuous-cast steel slab (0.203m x 1.321m) and can be easily converted into liquid steel flow rate through the nozzle (multiply by 0.203m x 1.321m to get

volume flow rate in m^3/s) or to casting speed for a different sized slab. Slide gate opening fraction F_L is a linear fraction of the opening distance. Argon is injected into the UTN at the "cold" flow rate Q_G measured at STP (Standard Temperature of 25˚C and Pressure of 1 atmosphere). The corresponding "hot" argon flow rate is used in the numerical simulation. This is because previous work has shown that the gas heats up to the steel temperature by the time it enters the nozzle [16]. The argon bubble size was fixed at 1 mm for all simulations. This is likely smaller than usually encountered in practice, but the effect on the pressure predictions should be negligible. Nozzle bore diameter D_N refers to the diameter of the circular opening in the slide-gate, which is assumed to be the same as the inner diameter of the SEN and bottom of the UTN. Decreasing D_N also approximates the effect of severe clogging when alumina builds up uniformly in the radial direction. Four different nozzle diameters are simulated in this work, 60-, 70-, 78-, and 90-mm. In order to isolate the effect of D_N and to better approximate uniform clogging buildup, all nozzles keep the same axial dimensions as the standard nozzle. The ports are proportionally scaled, however, to keep the same square shape for all bore sizes. The simulation conditions given in Table II cover a typical range of operating conditions used in practice.

Figure 3(a) shows a typical shaded contour plot of the pressure distribution in the standard nozzle from the 3-D finite-volume model simulation. Figure 3(b) shows the pressure profile along the nozzle, for a few different gate openings. The path follows the nozzle centerline from the nozzle top to point O at the center of the port section and then along the line from point O to the port outlet. It can be seen that the biggest pressure drop occurs across the slide gate, due to the throttling effect. The lowest pressure is found where the slide gate joins either the UTN or the SEN. Thus, joint sealing between the plates is very important to avoid air aspiration if a

vacuum occurs. Increasing gate opening results in smaller flow resistance and thus less pressure drop.

Flow through the nozzle is driven by gravity so the pressure at the top of the nozzle corresponds to the static pressure head in the tundish bath depth. Thus, the tundish bath depth, H_T, can be found from Bernoulli's equation, knowing the pressure-drop across the nozzle calculated in numerical simulation, Δp, the SEN submerged depth, H_{SEN}, and the weighted average liquid velocity at the top inlet of the nozzle port, U_B, and at the nozzle port, U_C,

$$H_T = \frac{\Delta p + \rho_l g H_{SEN} + \frac{1}{2}\rho_l (U_B^2 - U_C^2)}{\rho_l g} \tag{1}$$

The calculated tundish bath depths are plotted as a function of the other process variables in Figures 4(a-d). Each point in these plots is the result of a separate 3-D simulation.

C Multivariable Curve Fitting

In order to interpolate the results of the parametric study over a continuous range of operating conditions, equations were sought to curve-fit the data points generated with the 3-D computational flow model described in the previous section. Specifically, a multiple-variable curve fitting procedure was used to relate tundish bath depths to the other variables, This leads to a pair of linear equations containing 120 unknown constants. To obtain the values of these fitting constants, the least squares solution for the linear equations is then solved using the Normal Equation Method [20]. Derivation of the equations and their constants is detailed in Appendix A. The close match in Figures 4(a-d) between the lines generated from the derived equations and appropriate points from the computational model indicates the accuracy of this fit.

D. Inverse Models

For a given nozzle geometry and clogging status, the five basic casting process variables: casting speed, argon injection flow rate, gate opening, nozzle diameter and tundish bath depth are related. Choosing values for any four of these variables intrinsically determines the fifth.

The plots in Figure 4 are inconvenient to interpret in practice because the tundish bath depth is usually kept constant during a stable continuous casting process. To present the results in arbitrary practical ways, tundish bath depth was transformed from a dependent to an independent variable. Specifically, Equation A2 is inverted into four other forms with either V_C, Q_G, D_N or F_L as the dependent variable, as shown in Appendix B. These "inverse models" can then be used to study relationships between the process variables. Figures 5 and 6 show typical plots with two of the inverse models.

The following observations can be made from examination of Figures 4-6:

- For a given nozzle geometry and gas flow rate, casting speed increases with a deeper tundish bath depth (constant gate opening) or a larger gate opening (constant bath depth).
- Casting speed is more sensitive to a given change in tundish bath depth at shallow bath depth than at deep bath depth.
- Casting speed is more sensitive to a change in bath depth at large gate opening than at small gate opening.
- Casting speed is more sensitive to gate opening when maintaining a high casting speed.
- Steel flow rate is more sensitive to gate opening changes when the gate opening is near either 50% or 100%
- For a given tundish bath depth, increasing argon injection will slow down the casting speed slightly unless the gate opening increases to compensate.

- For a given gas flow rate, the gas fraction increases greatly at low casting speeds, resulting in large buoyancy forces which reduce the effectiveness of the gate opening and makes it difficult even to drain the tundish.
- The extent of clogging can be inferred by comparing the measured steel flow rate with that of the inverse model for a given nozzle geometry, tundish bath depth, gas flow rate gate opening fraction.

E. Combined Model

The same multivariable curve-fitting method used to fit data for tundish bath depth (Equation A1) can be employed to develop equations for other important nozzle flow characteristics under practical operating conditions. Such characteristics include the lowest pressure in the nozzle (air aspiration), bias flow due to the slide-gate throttling, and the properties of the jets exiting the nozzle ports.

For this work, equations are now developed to predict the lowest pressure in the nozzle. When the lowest pressure in nozzle is below atmospheric pressure, air aspiration may occur if the joints are not properly sealed. In the 3-D numerical simulations, the reference ambient pressure is set to zero. Therefore, a negative pressure predicted in the simulation implies the existence of a partial vacuum (less than one atmosphere) which suggests a tendency for air aspiration, if there is any porosity, leaks, or cracks in the nozzle.

For each 3-D simulation case in Table II, the lowest pressure in the nozzle is recorded. The results are then curve-fit to produce an equation for the lowest pressure, P_L, as a function of the four independent variables, V_C, F_L, Q_G, and D_N. As shown in Figure 7, the V_C dependence fits well with a quadratic function, Q_G fits well with a linear function, D_N fits well with a cubic function, and F_L must be split into two different linear regions for $F_L \leq 70\%$ and $F_L \geq 70\%$. The overall relationship can be written as

$$P_L = \left(b_1 V_C^2 + b_2 V_C + b_3\right)\left(b_4 F_L + b_5\right)\left(b_6 Q_G + b_7\right)\left(b_8 D_N^3 + b_9 D_N^2 + b_{10} D_N + b_{11}\right)$$

$$\text{for} \quad F_L \le 70\% \qquad (2a)$$

$$P_L = \left(b_{12} V_C^2 + b_{13} V_C + b_{14}\right)\left(b_{15} F_L + b_{16}\right)\left(b_{17} Q_G + b_{18}\right)\left(b_{19} D_N^3 + b_{20} D_N^2 + b_{21} D_N + b_{22}\right)$$

$$\text{for} \quad F_L \ge 70\% \qquad (2b)$$

where the b_i (i=1-22) are unknown constants. As with Equations A1, Equations 2 are expanded to yield a new pair of linear equations which contains 96 new fitting constants, as detailed elsewhere [21]. These new fitting constants are solved using the same least square curve fitting procedure as for Equations A2.

The close match in Figures 7(a-d) between the lines from Equations 2 and appropriate points from the computational model indicates the accuracy of this fit. Using two different linear functions to fit the P_L *vs*. F_L data produces the sharp transitions at F_L=70% in Figure 7(d). A smoother transition would likely be obtained if more data between F_L=70% and F_L=100% were generated and a higher-order fitting model were employed for P_L *vs*. F_L.

It should be cautioned that all of the curves in Figures 7(a-d) correspond to varying tundish bath depths. This makes this presentation of the results difficult to interpret. In practice, the tundish bath depth is usually kept at a relatively constant level. It is the gate opening that is continuously adjusted to compensate for changes in the other variables, such as clogging and gas flow rate in order to maintain a constant casting speed. To better present the minimum pressure results in Equation 2 under these practical conditions, it is combined with one of the inverse models derived in Appendix B. Specifically, the inverse model for F_L as a function of V_C, H_T, Q_G, and D_N is simply inserted to replace F_L in Equations 2. This yields the combined model expressing P_L as a function of these four practical independent variables. The results are presented in Section V.

III. MODEL VALIDATION WITH PLANT MEASUREMENTS

To verify the curve-fit model and the corresponding inverse model, the predictions from the inverse model are compared with measurements on an operating steel slab casting machine. Using Validation Nozzle A in Table I, gate opening positions were recorded for different steel throughputs over several months [22]. Figure 8 shows the several thousand data points thus obtained. Only first heats in a sequence were recorded in order to minimize the effect of clogging. The tundish bath depth was held constant (H_T=1.125m) for these data, and the argon injection ranged from 7 to 10 SLPM. Since the measurements were recorded with different units from the Table II for the inverse model, the model predictions require conversion of F_L to the plant definition of gate opening F_P and casting speed to steel throughput Q_{Fe} by

$$F_P = (1\text{-}24\%)F_L + 24\% \tag{3}$$

and

$$Q_{Fe}(tonne/min)=1.8788\ V_C(m/min) \tag{4}$$

The geometry of the Validation Nozzle A is not exactly the same as the standard nozzle on which the inverse model predictions are based, but it is reasonably close. In addition to the inverse model prediction, additional 3-D finite-volume model simulations were performed for the actual geometry of the Validation Nozzle A in Table I. These results also are shown in Figure 8 as three big dots.

Figure 8 shows that the 3-D simulation results are very close to the inverse model predictions, despite the slight difference in nozzle geometry. In addition to validating both models, this suggests that the inverse model derived from the standard nozzle is applicable to other practical conditions, if the nozzle geometry is reasonably close. This is due to the fact that the pressure drop across the nozzle depends mainly on the flow resistance. Port design greatly

affects the jet properties exiting the nozzle [23], but has little effect on the pressure drop of most concern to this prediction.

Both the predictions from the inverse model and the CFX simulation match the larger extreme of the range of measured gate opening percentage in Figure 8 for a given steel throughput. The decreased gate opening often experienced in the plant is likely due to the following reasons:

- Less argon flow in the plant (7-10 SLPM vs. 10 SLPM) needs smaller openings to accommodate the same liquid flow.
- Incomplete bubbly flow or K-ε turbulence model uncertainty might be another source for lack of fit.
- Rounded edges likely found in the plant nozzles may cause less pressure drop than the sharp edge in new or simulated nozzles, so need less opening to achieve the same flow.
- The initial clogging experienced during the first heat may reduce the gate opening required for a given steel throughput. This is because, before it starts to restrict the flow channel, the streamlining effect of initial clogging may reduce the overall pressure loss across nozzle. The last two factors will be discussed further in the next section.

IV. EFFECT OF CLOGGING

A. Initial Clogging and Edge Sharpness

In both numerical simulations and experiments, three recirculation zones are observed in the vicinity of the slide-gate [16, 24]. One forms in the cavity of the slide-gate itself and the other two are located just above and below the throttling plate. In these recirculation zones, the flow is turbulent and the gas concentration is high. These recirculation zones and the sharp edges of the slide gate surfaces both may create an extra resistance to flow. Slight erosion by the flowing steel may round off the ceramic corners. In addition, it is known that clogging tends to buildup

initially in the recirculation regions [24]. Because of this, the initial clogging might not impede the flow and instead may decrease the flow resistance by streamlining the flow path. This may decrease the total pressure drop across the nozzle.

To investigate these phenomena, four simulations were performed using the 3-D finite volume model for the cases illustrated in Figure 9. The geometry and casting conditions, given in Table I for Validation Nozzle B, were chosen to match conditions where measurements were available for comparison [25]. All four cases are the same, except for the geometry near the slide gate. The first case, Figure 9(a) has sharp edges similar to the standard nozzle simulated in the foregoing parametric study. The next case, shown in Figure 9(b), has the four slide gate edges rounded with a 3mm radius. The final two cases have the recirculation regions partially filled in to represent two different amounts of initial clogging with alumina reinforced by solidified steel. The case in Figure 9(c) has solid clog material in the gate cavity and around the throttling gate and smooth surfaces in the upper SEN. The final case, Figure 9(d), has extra clogging at the same places but with more buildup around the gate.

Figure 10 shows the simulated flow pattern at the center plane parallel to the mold narrow face. Differences such as edge roundness and clogging around the slide gate greatly change both the flow pattern in the SEN and the jets out of the ports. The jets are seen to vary from two small symmetric swirls to a single large swirl which can switch rotational directions. Thus, a slight change in clogging can suddenly change the jet characteristics exiting the port.

The clogging condition and edge roundness affects not only the flow pattern, but also the pressure drop across the nozzle. From the numerical simulation results, the corresponding tundish bath depth for each case was calculated using Equation 1. These values are compared in Figure 11 with the measured tundish bath depth. The standard sharp-edge case with no clogging has the largest pressure drop, so requires the greatest bath depth. Rounding the edges of the

throttling plates reduces the pressure drop across the gate plates and lowers the required tundish head by 18%. Initial clogging is even more effective at streamlining the liquid steel flow around the slide-gate, as it decreases the recirculation zones and lowers the pressure drop. The initial clogging of Figure 11(c) reduces the required tundish bath depth by 24%, relative to the standard sharp, non-clogged case. Further initial clogging, case Figure 11(d), decreases the required tundish bath depth by 36%, which is lower than the measured value of 0.927m. The measurement was taken during the first heat, so only initial clogging buildup is possible. Given the demonstrated importance of this initial buildup, the simulation is consistent with the uncertain measurement conditions.

The extent of these pressure drop variations caused by clogging is very significant to steel quality. To compensate for these pressure variations, the position of flow control device (slide gate or stopper rod) must change. Because mass flow from the nozzle ports changes with the extent of the flow restriction, this compensation will produce transient flow asymmetry in the mold. Together with the inherent changes in velocities exiting the ports, this will produce transient fluctuations in flow and level in the mold cavity which have been observed in practice [4]. These results provide strong evidence for the quality problems caused by initial nozzle clogging.

B. Severe Clogging

With increasing alumina buildup, the clogging, instead of streamlining the flow, begins to restrict the flow channel and to create extra flow resistance. The gate opening then must increase to maintain constant liquid steel flow rate through the nozzle. The effect of clogging on the flow depends on both how much alumina is deposited and the clogging shape (where and how the alumina deposits). Clogging often builds up relatively uniformly in the radial direction and acts to reduce the diameter of the nozzle bore [1, 13]. The effect of this type of clogging is similar to the

effect of reducing the bore diameter. Figure 4(c) shows that decreasing the bore size, (or increasing clogging), requires the tundish liquid level to increase in order to maintain the same flow rate at a constant gate opening. Using the inverse model, the effect of clogging/decreasing bore size is quantified in Figure 12, for the more practical condition of constant tundish level.

Figure 12(a) shows how gate opening must increase to accommodate clogging (or decreasing bore size) in order to maintain a constant flow rate for a fixed tundish level. It can be seen that the gate opening is much less sensitive to clogging when the bore diameter is large. Thus, clogging may be difficult to detect from gate changes until it is very severe and the gate opening fraction increases (above 60% for the condition here). Figure 12(b) shows how the steel flow rate decreases if the gate opening percentage does not change.

V. AIR ASPIRATION

If pressure in the nozzle falls below one atmosphere, then air may aspirate through joints, cracks, or porosity in the nozzle ceramic, leading to reoxidation and clogging. One of the suggested mechanisms for the beneficial effect of argon injection in reducing nozzle clogging is that the argon generates positive pressure in the nozzle [14]. Numerical simulations in this work, Figure 7, and water modeling [14] both show that the minimum pressure in the nozzle can drop below zero in some circumstances, and that argon gas injection can raise that pressure above zero.

The lowest pressure in the nozzle is also affected by the casting speed, gate opening, tundish bath depth, and nozzle bore size (or extent of clogging), as shown in Figure 7. The combined fitting model (Equation 2) is now applied to study the effects of these variables on minimum pressure. The lowest pressure in the nozzle is generally found just below the slide gate. When the pressure drop across the gate is small and there is no vacuum problem (e.g., when the

gate is almost full open), the minimum pressure in the nozzle moves to the nozzle ports. The port pressure depends mainly on SEN submergence depth.

The minimum pressure is presented as a function of casting speed in Figures 13 for different argon injection rates and nozzle bore sizes and as a function of argon flow rate in Figures 14 for different casting speeds. All of these figures fix the tundish bath depth and allow gate opening to vary, which reflects practical operation conditions. The corresponding gate openings, along with both "cold" and "hot" argon injection volume fractions, are also marked on Figures 13-14 for easy reference.

A. Effect of Argon Flow Rate

The results in Figures 7, 13 and 14 quantify how increasing argon flow rate tends to decrease the pressure drop across the slide gate, thereby raising the minimum pressure in the nozzle and making air aspiration less likely. Figures 14 show that the main reason for this is the increased opening of the gate that is needed to compensate for the gas volume in order to maintain the liquid flow rate.

B. Effect of Tundish Bath Depth

Decreasing tundish bath depth is shown to decrease the pressure drop across the slide gate if the gate opening is unchanged, thereby raising the minimum pressure in the nozzle and making air aspiration less likely. In general, lowering the total pressure head by any means is beneficial for reducing reoxidation problems.

C. Effect of Casting Speed

The effect of casting speed is complicated because of several competing effects. Higher liquid flow rate tends to increase the pressure drop and vacuum problems. At the same time, increasing the flow rate allows the gate to open wider, which tends to alleviate the vacuum problems. The worst vacuum problems occur with the gate at about 60% open by distance or

50% open by area fraction, regardless of casting speed (see Figures 13). Above 70% linear gate opening, the effect of decreasing the throttling effect with increased gate opening dominates, so that the vacuum problems are reduced with increasing casting speed. Below 50% gate opening, the effect of lowering casting speed dominates, so that the vacuum problems are reduced with decreasing speed. A further effect that helps to reduce vacuum problems at lower casting speed is that the gas percentage increases (for a fixed gas flow rate).

D. Effect of Bore Diameter

The common practice of employing oversized nozzle bores to accommodate some clogging forces the slide gate opening to become more restricted. This makes the opening fraction smaller, so aspiration problems due to vacuum problems generally increase with increasing bore size. This trend is consistent for opening fractions above 50%, as seen by comparing Figures 13 (b) and (c). However, the actual opening area may increase slightly, which tends to reduce vacuum problems. Thus the net effect of bore diameter is not consistent when the linear opening fraction is less than 50%.

VI. OPTIMIZING ARGON FLOW

Injecting argon gas sometimes enables the transition from an air aspiration condition to positive pressure in the nozzle. The minimum argon flow rate required to avoid any vacuum in the nozzle can be obtained by letting P_L=0 in Equation 2 and solving for Q_G. The results are plotted in Figures 15 as a function of casting speed at fixed tundish bath depth for two different nozzle bore sizes. The top of these figures shows the corresponding slide gate opening fraction. The results suggest how to optimize argon flow to avoid air aspiration conditions in the nozzle.

The minimum argon flow rate required to avoid a vacuum condition can be read from Figures 15. It increases greatly with tundish bath depth. For a given tundish bath depth, the

minimum argon flow rate first increases rapidly with increasing casting speed, and then decreases with increasing casting speed. The most argon is needed for linear gate openings between 50%-70% for the reasons discussed in Section V. C.

At low casting speed, (below 0.5m/min), or at low tundish levels (below 0.6m), no vacuum is predicted in the nozzle. Thus, argon injection is not needed to prevent air aspiration under these conditions. During ladle transitions and at other times when either casting speed or tundish level is low, argon flow rate should be severely reduced and chosen according to other criteria. Besides saving argon, this avoids flow problems in the mold and defects due to possible gas bubble entrapment.

For high tundish level (deeper than 1.2m) and high casting speed (above 1.5m/min), Figures 15 show that very large argon flow rates (over 20 SLPM) are needed to avoid a vacuum condition. Specifically, a 0.2m increase in tundish bath depth typically requires an additional 5 SLPM of argon to compensate the vacuum effect at high casting speeds. In practice, the argon injection flow rate is limited to a maximum of about 15 SLPM (or 20% gas volume fraction, which corresponds to less than 5% gas at STP). This is because argon injection greatly changes the flow pattern in the mold [26]. Excessive argon injection also may cause a transition from "bubbly flow" to "annular" flow in the nozzle [27], create boiling action at the meniscus and cause quality problems [13]. Therefore, it is not feasible for argon injection to eliminate the vacuum in the nozzle when the tundish bath is deep and the casting speed is high. Other steps should be taken to avoid air aspiration for these conditions. Besides improving the sealing at the joints (especially the joints between the slide-gate, the lower plate, and the SEN holder), other methods suggested by the model (Equation 2) include:

- Choose bore diameters according to the steel flow rate in order to avoid linear gate openings near 60%. To increase gate openings above 60%, a smaller nozzle bore

diameter could be used, although this allows little accommodation for clogging. To decrease gate openings to below 60%, a larger bore diameter is needed.

- Decrease tundish bath depth or lower the tundish. A lower tundish level creates less pressure drop, so generates less vacuum tendency.

Finally, it must be noted that clogging can be alleviated in many ways other than by argon injection [1]. Moreover, argon gas can act to prevent clogging in several other ways [1]. Very high gas flow rates can form a gas film that prevents molten steel contact with the nozzle walls [28]. Argon gas generates flow turbulence that can dislodge delicate inclusion formations from the nozzle walls. Gas bubbles attach to inclusions and transport them through the nozzle. Finally, argon may retard the chemical reactions between the steel and refractory that causes some types of clogs. In addition to the effect of argon on reduction of air aspiration-reoxidation-based clogs studied in this work, these other mechanisms should be quantitatively investigated in future work and considered when optimizing argon gas injection.

VII. CONCLUSIONS

The turbulent flow of liquid steel and argon bubbles in a slide-gate nozzle has been simulated with a verified three-dimensional finite volume model. The results are further processed using multivariable curve fitting methods to relate casting speed, argon injection rate, slide-gate opening position, nozzle bore diameter and tundish bath depth to clogging and air aspiration potential.

Both smoothing the nozzle edges due to erosion and initial clogging buildup are found to enhance the steel flow rate due to a streamlining effect. Only after severe clogging builds up is the flow eventually restricted so that the gate opening must increase to maintain the casting speed. In addition, both initial clogging and edge smoothing can greatly affect the flow pattern

and jet characteristics. The extent of clogging can be inferred by comparing the measured steel flow rate to the model predictions, leading to a "clogging index".

The pressure drop generated across the partially-closed slide gate may create a partial vacuum near the slide gate which tends to entrain air, leading to reoxidation problems. The worst vacuum appears to occur for 50%-70% linear gate opening (about 50% area fraction). Increasing argon injection helps to raise the lowest pressure and sometimes is sufficient to avoid this vacuum. For shallow tundish bath depths or low casting speeds, the pressure is always positive, so argon is not needed for this purpose. Less argon is needed if the nozzle bore size is chosen to avoid intermediate casting speeds so that the gate is either nearly fully open or is less than 50%. For high casting speeds, a 0.2m increase in tundish bath depth typically will require on the order of an additional 5 SLPM of argon to compensate the vacuum effect. In practice, argon injection is limited by its effect on the flow pattern, and is often unable to fully avoid the vacuum effect.

ACKNOWLEDGMENTS

The authors wish to thank the National Science Foundation (Grant #DMI-98-00274) and the Continuous Casting Consortium at UIUC, including Allegheny Ludlum, (Brackenridge, PA), Armco Inc. (Middletown, OH), Columbus Stainless (South Africa), Inland Steel Corp. (East Chicago, IN), LTV Steel (Cleveland, OH), and Stollberg, Inc., (Niagara Falls, NY) for their continued support of our research, AEA technology for use of the CFX4.2 package and the National Center for Supercomputing Applications (NCSA) at the UIUC for computing time. Additional thanks are extended to researchers at LTV Steel and Inland Steel for providing plant data and feedback.

APPENDIX A:

CURVE-FITTING EQUATIONS FOR TUNDISH BATH DEPTH

Equations to relate tundish bath depths (H_T) with other operating variables (casting speed $V_{C,}$ argon flow rate Q_G, slide gate opening fraction F_L and nozzle bore diameter D_N) are obtained by fitting the points which are generated with the computational model, using a multiple-variable curve fitting procedure. First, the form of the equation is chosen for each variable. Figure 4(a) shows that the H_T *vs*. V_C data fits well with a quadratic polynomial function. The H_T *vs*. Q_G data shown in Figure 4(b) is linear, and the H_T *vs*. D_N data in Figure 4(c) fits well with a cubic function. A single simple function could not be found to fit the H_T *vs*. F_L data in Figure 4(d) over the whole F_L range. Thus, these data were split into two regions, with a quadratic function for $F_L \le 60\%$ and a linear function for $F_L \ge 60\%$. Together, the overall relation is:

$$H_T = \left(a_1 V_C^2 + a_2 V_C + a_3\right)\left(a_4 F_L^2 + a_5 F_L + a_6\right)\left(a_7 Q_G + a_8\right)\left(a_9 D_N^3 + a_{10} D_N^2 + a_{11} D_N + a_{12}\right)$$

$$\text{for} \quad F_L \le 60\% \qquad \text{(A1a)}$$

$$H_T = \left(a_{13} V_C^2 + a_{14} V_C + a_{15}\right)\left(a_{16} F_L + a_{17}\right)\left(a_{18} Q_G + a_{19}\right)\left(a_{20} D_N^3 + a_{21} D_N^2 + a_{22} D_N + a_{23}\right)$$

$$\text{for} \quad F_L \ge 60\% \qquad \text{(A1b)}$$

where the a_i are 23 unknown constants. Each numerical simulation case generates one data point (H_T, V_C, F_L, Q_G, D_N) to help find the constants in this equation.

Because the number of simulation cases (Table II) exceeds the number of unknown coefficients, an optimization was needed to obtain the best fit. However, Equations A1 are nonlinear equations, so are difficult to optimize. Thus, Equations A1 were expanded to the following pair of linear equations which contain 120 unknown constants, c_i,

$$H_T = c_1 + c_2 V_C + c_3 F_L + c_4 Q_G + c_5 V_C F_L + c_6 V_C Q_G + c_7 F_L Q_G + c_8 V_C F_L Q_G + c_9 V_C^2 + c_{10} F_L^2$$

$$+ \; c_{11} V_C F_L^2 + c_{12} V_C^2 F_L + c_{13} V_C^2 Q_G + c_{14} F_L^2 Q_G + c_{15} V_C^2 F_L^2 + c_{16} V_C F_L^2 Q_G$$

$$+ c_{17}V_C^2F_LQ_G + c_{18}V_C^2F_L^2Q_G$$

$$+ c_{19}D_N + c_{20}V_CD_N + c_{21}F_LD_N + c_{22}Q_GD_N + c_{23}V_CF_LD_N + c_{24}V_CQ_GD_N + c_{25}F_LQ_GD_N$$

$$+ c_{26}V_CF_LQ_GD_N + c_{27}V_C^2D_N + c_{28}F_L^2D_N$$

$$+ c_{29}V_CF_L^2D_N + c_{30}V_C^2F_LD_N + c_{31}V_C^2Q_GD_N + c_{32}F_L^2Q_GD_N + c_{33}V_C^2F_L^2D_N + c_{34}V_CF_L^2Q_GD_N$$

$$+ c_{35}V_C^2F_LQ_GD_N + c_{36}V_C^2F_L^2Q_GD_N$$

$$+ c_{37}D_N^2 + c_{38}V_CD_N^2 + c_{39}F_LD_N^2 + c_{40}Q_GD_N^2 + c_{41}V_CF_LD_N^2 + c_{42}V_CQ_GD_N^2 + c_{43}F_LQ_GD_N^2$$

$$+ c_{44}V_CF_LQ_GD_N^2 + c_{45}V_C^2D_N^2 + c_{46}F_L^2D_N^2$$

$$+ c_{47}V_CF_L^2D_N^2 + c_{48}V_C^2F_LD_N^2 + c_{49}V_C^2Q_GD_N^2 + c_{50}F_L^2Q_GD_N^2 + c_{51}V_C^2F_L^2D_N^2 + c_{52}V_CF_L^2Q_GD_N^2$$

$$+ c_{53}V_C^2F_LQ_GD_N^2 + c_{54}V_C^2F_L^2Q_GD_N^2$$

$$+ c_{55}D_N^3 + c_{56}V_CD_N^3 + c_{57}F_LD_N^3 + c_{58}Q_GD_N^3 + c_{59}V_CF_LD_N^3 + c_{60}V_CQ_GD_N^3 + c_{61}F_LQ_GD_N^3$$

$$+ c_{62}V_CF_LQ_GD_N^3 + c_{63}V_C^2D_N^3 + c_{64}F_L^2D_N^3$$

$$+ c_{65}V_CF_L^2D_N^3 + c_{66}V_C^2F_LD_N^3 + c_{67}V_C^2Q_GD_N^3 + c_{68}F_L^2Q_GD_N^3 + c_{69}V_C^2F_L^2D_N^3 + c_{70}V_CF_L^2Q_GD_N^3$$

$$+ c_{71}V_C^2F_LQ_GD_N^3 + c_{72}V_C^2F_L^2Q_GD_N^3$$

for $F_L \le 60\%$ (A2a)

$$H_T = c_{73} + c_{74}V_C + c_{75}F_L + c_{76}Q_G + c_{77}V_CF_L + c_{78}V_CQ_G + c_{79}F_LQ_G$$

$$+ c_{80}V_CF_LQ_G + c_{81}V_C^2 + c_{82}V_C^2F_L + c_{83}V_C^2Q_G + c_{84}V_C^2F_LQ_G$$

$$+ c_{85}D_N + c_{86}V_CD_N + c_{87}F_LD_N + c_{88}Q_GD_N + c_{89}V_CF_LD_N + c_{90}V_CQ_GD_N + c_{91}F_LQ_GD_N$$

$$+ c_{92}V_CF_LQ_GD_N + c_{93}V_C^2D_N + c_{94}V_C^2F_LD_N + c_{95}V_C^2Q_GD_N + c_{96}V_C^2F_LQ_GD_N$$

$$+ c_{97}D_N^2 + c_{98}V_CD_N^2 + c_{99}F_LD_N^2 + c_{100}Q_GD_N^2 + c_{101}V_CF_LD_N^2 + c_{102}V_CQ_GD_N^2 + c_{103}F_LQ_GD_N^2$$

$$+ c_{104}V_CF_LQ_GD_N^2 + c_{105}V_C^2D_N^2 + c_{106}V_C^2F_LD_N^2 + c_{107}V_C^2Q_GD_N^2 + c_{108}V_C^2F_LQ_GD_N^2$$

$$+ c_{109}D_N^3 + c_{110}V_C D_N^3 + c_{111}F_L D_N^3 + c_{112}Q_G D_N^3 + c_{113}V_C F_L D_N^3 + c_{114}V_C Q_G D_N^3 + c_{115}F_L Q_G D_N^3$$

$$+ c_{116}V_C F_L Q_G D_N^3 + c_{117}V_C^2 D_N^3 + c_{118}V_C^2 F_L D_N^3 + c_{119}V_C^2 Q_G D_N^3 + c_{120}V_C^2 F_L Q_G D_N^3$$

$$\text{for} \quad F_L \geq 60\% \qquad \text{(A2b)}$$

The least square solution for the linear equations is then solved for the 120 coefficients using the Normal Equation Method [20], which minimizes the sum of the squares of the distances of each data point from the fitting curve. The fitting constants obtained for the standard nozzle in Table I and the simulation condition in Table II are summarized in Table III.

Table III. Values of the fitting constants in Equation A2

$c_1 - c_{30}$	$c_{31} - c_{60}$	$c_{61} - c_{90}$	$c_{91} - c_{120}$
1.30825E+01	3.04846E-02	-9.72287E-08	9.21830E-05
-4.69344E+00	2.77463E-05	4.86029E-07	-9.58526E-05
-2.49016E-01	-1.62408E-03	-2.82577E-04	-5.65170E-01
2.99228E-02	-1.08873E-04	-3.53295E-09	5.18189E-03
2.73630E-01	-1.75721E-03	4.68209E-09	1.75703E-03
8.03658E+00	2.00511E-05	8.77755E-06	-3.45058E-05
6.79806E-02	4.86635E-03	1.33099E-06	2.89135E-03
-3.39823E-01	-1.74584E-03	1.21144E-09	-1.09581E-03
1.97573E+02	-9.26275E-05	-7.09090E-08	-3.89911E-06
2.47017E-03	1.11305E-05	-4.75351E-09	4.38101E-04
-3.27363E-03	1.01783E-04	-7.67217E-08	1.37908E-05
-6.13711E+00	2.98941E-03	8.75451E-10	-1.54152E-04
-9.30606E-01	2.52870E-05	7.77298E+00	-1.04677E-06
-8.47014E-04	-1.26405E-04	-2.94592E+00	1.08843E-06
4.95783E-02	7.34920E-02	-1.04822E-02	6.41767E-03
3.32357E-03	9.18842E-07	1.17777E+00	-5.88419E-05
5.36424E-02	-1.21771E-06	3.70745E-02	-1.99515E-05
-6.12100E-04	-2.28285E-03	-4.14416E-01	3.91824E-07
-4.28553E-01	-3.46162E-04	-2.81409E-03	-1.11172E-05
1.53747E-01	-3.15068E-07	2.92610E-03	4.21339E-06
8.15721E-03	1.84419E-05	1.72530E+01	1.49921E-08
-9.80206E-04	1.23628E-06	-1.58188E-01	-1.68450E-06
-8.96352E-03	1.99536E-05	-5.36368E-02	-5.30255E-08
-2.63261E-01	-2.27686E-07	1.05336E-03	5.92716E-07
-2.22690E-03	-1.87111E-05	-2.54626E-01	4.02483E-09
1.11319E-02	6.71276E-06	9.65021E-02	-4.18503E-09
-6.47205E+00	3.56153E-07	3.43374E-04	-2.46760E-05
-8.09176E-05	-4.27969E-08	-3.85812E-02	2.26247E-07
1.07237E-04	-3.91357E-07	-1.21448E-03	7.67137E-08
2.01038E-01	-1.14943E-05	1.35754E-02	-1.50656E-09

APPENDIX B: INVERSE MODEL DERIVATION

In order to transform tundish bath depth from a dependent in Equation A2 to an independent variable, Equation A2 is inverted into four other forms with either V_C, Q_G, D_N or F_L as the dependent variable. For the example of fixed tundish bath depth (H_T), fixed gate opening (F_L) less than 60%, fixed nozzle diameter (D_N), and fixed argon injection flow rate (Q_G), Equation A2a can be rewritten as:

$$aV_C^2 + bV_C + c = 0 \tag{B1}$$

where

$$\begin{aligned} a = {} & c_9 + c_{12}F_L + c_{13}Q_G + c_{15}F_L^2 + c_{17}F_LQ_G + c_{18}F_L^2Q_G \\ & + c_{27}D_N + c_{30}F_LD_N + c_{31}Q_GD_N + c_{33}F_L^2D_N + c_{35}F_LQ_GD_N + c_{36}F_L^2Q_GD_N \\ & + c_{45}D_N^2 + c_{48}F_LD_N^2 + c_{49}Q_GD_N^2 + c_{51}F_L^2D_N^2 + c_{53}F_LQ_GD_N^2 + c_{54}F_L^2Q_GD_N^2 \\ & + c_{63}D_N^3 + c_{66}F_LD_N^3 + c_{67}Q_GD_N^3 + c_{69}F_L^2D_N^3 + c_{71}F_LQ_GD_N^3 + c_{72}F_L^2Q_GD_N^3 \end{aligned} \tag{B2a}$$

$$\begin{aligned} b = {} & c_2 + c_5F_L + c_6Q_G + c_{11}F_L^2 + c_8F_LQ_G + c_{16}F_L^2Q_G \\ & + c_{20}D_N + c_{23}F_LD_N + c_{24}Q_GD_N + c_{29}F_L^2D_N + c_{26}F_LQ_GD_N + c_{34}F_L^2Q_GD_N \\ & + c_{38}D_N^2 + c_{41}F_LD_N^2 + c_{42}Q_GD_N^2 + c_{47}F_L^2D_N^2 + c_{44}F_LQ_GD_N^2 + c_{52}F_L^2Q_GD_N^2 \\ & + c_{56}D_N^3 + c_{59}F_LD_N^3 + c_{60}Q_GD_N^3 + c_{65}F_L^2D_N^3 + c_{62}F_LQ_GD_N^3 + c_{70}F_L^2Q_GD_N^3 \end{aligned} \tag{B2b}$$

$$\begin{aligned} c = {} & c_1 + c_3F_L + c_4Q_G + c_{10}F_L^2 + c_7F_LQ_G + c_{14}F_L^2Q_G - H_T \\ & + c_{19}D_N + c_{21}F_LD_N + c_{22}Q_GD_N + c_{28}F_L^2D_N + c_{25}F_LQ_GD_N + c_{32}F_L^2Q_GD_N \\ & + c_{37}D_N^2 + c_{39}F_LD_N^2 + c_{40}Q_GD_N^2 + c_{46}F_L^2D_N^2 + c_{43}F_LQ_GD_N^2 + c_{50}F_L^2Q_GD_N^2 \\ & + c_{55}D_N^3 + c_{57}F_LD_N^3 + c_{58}Q_GD_N^3 + c_{64}F_L^2D_N^3 + c_{61}F_LQ_GD_N^3 + c_{68}F_L^2Q_GD_N^3 \end{aligned} \tag{B2c}$$

The theoretical casting speed is then obtained from:

$$V_C = \frac{-b + \sqrt{b^2 - 4ac}}{2a} \qquad \text{for} \quad F_L \le 60\% \qquad \text{(B3)}$$

The other root is always negative, which is physically incorrect. Similar equations are derived and detailed elsewhere for gate openings greater than 60% and for F_L, Q_G, or D_N as the dependent variables [21].

NOMENCLATURE

a_i, b_i, c_i, d_i	curve fitting constants
D_N	diameter of nozzle bore (mm)
F_A	slide-gate opening (area fraction, Equation 1)
F_L	slide-gate opening, linear fraction
f_g	gas volume fraction ("hot" argon in steel)
g	gravitational acceleration (9.81m/s^2)
H_T	tundish bath depth (m)
H_{SEN}	SEN submerged depth (m)
P_L	lowest pressure in nozzle (kPa)
Q_G	"cold" argon gas flow rate, measured at standard conditions (STP of 25˚C and 1 atmosphere pressure) (SLPM)
Q_{Fe}	steel throughput (tonne/min)
U_B	average velocity at the top inlet of the nozzle (m/s)
U_C	average jet velocity at the nozzle port (m/s)
V_C	casting speed based on 0.203m x 1.321m slab (m/min)

FIGURE CAPTIONS

Figure 1. Computational domain and boundary conditions for the standard nozzle

Figure 2. Simulated flow field for the standard nozzle and conditions in Table I
(a) Argon gas distribution (b) Velocities in center plane parallel to WF
(c) Velocities in center plane parallel to NF (d) Velocities at port outlet plane

Figure 3. Pressure distribution in the standard nozzle, predicted by the 3-D finite difference model (a) shaded contour plot at the center-plane (b) pressure profile along the centerline (from top to outlet port)

Figure 4 CFX model output (points from Equation 1) and fitting curve (lines of Equation A2) showing effects of casting speed, gate opening, argon injection and nozzle bore size

Figure 5 Inverse model plots showing effect of gate opening and tundish bath depth on casting speed (a) No gas injection (b) 5 SLPM argon injection

Figure 6. Inverse model plots showing effect of gas injection and tundish bath depth on casting speed

Figure 7. CFX model output (points) and fitting curve (lines of Equations 2) showing effects of casting speed, gate opening, argon injection and nozzle bore size on the lowest pressure P_L in nozzle (under varying tundish bath depth)

Figure 8. Comparison of measured and model predicted relationship between opening restriction fraction and steel flow rate (Validation Nozzle A)

Figure 9. Assumed shape of initial clogging and rounded edges in the vicinity of the slide-gate (Validation Nozzle B)

Figure 10. Effects of initial clogging and rounded edges on nozzle flow pattern
(center plane parallel to the narrow face for Validation Nozzle B)

Figure 11. Effects of initial clogging and rounded edges on predicted tundish bath depth
(Validation Nozzle B)

Figure 12. Effects of change in nozzle bore size (such as caused by clogging)

Figure 13 Effect of casting speed on minimum pressure in the nozzle for constant tundish bath depth and argon injection flow rate (a) 10 SLPM argon injection, 78 mm nozzle bore (b) 5 SLPM argon injection, 78 mm nozzle bore (c) 5 SLPM argon injection, 70 mm nozzle bore

Figure 14 Effect of argon injection flow rate on minimum pressure in the nozzle for constant tundish bath depth and casting speed (a) 1 m/min casting speed, 78 mm nozzle bore (b) 1.5 m/min casting speed, 78 mm nozzle bore

Figure 15. Effect of casting speed and tundish depth on minimum argon flow rate required for positive pressure in nozzle (bottom) and the corresponding gate opening (top) (a) 78 mm nozzle bore (b) 70 mm nozzle bore

REFERENCES

1. K.G. Rackers and B.G. Thomas: "Clogging in Continuous Casting Nozzles", in *78th Steelmaking Conference*, vol. 78, (Nashville, TN, April 2-5, 1995), ISS, Warrendale, PA, 1995, pp. 723-34.

2. F.L. Kemeny: "Tundish Nozzle Clogging - Measurement and Prevention", in *McLean Symposium Proceedings*, (Toronto, Ontario, March 22-25, 1998), ISS, Warrendale, PA, 1998, pp. 103-10.

3. B.G. Thomas and H. Bai: "Tundish Nozzle Clogging – Application of Computational Models", in *Steelmaking. Conf. Proc*., vol. 84, (18th PTD Conf., Baltimore, MD, March 25-28), Iron and Steel Society, Warrendale, PA, 2001, pp. 895-912.

4. M. Milone, Winke and I. Samarasekera: "Meniscus Thermal Analysis as a Tool for Evaluating Slab Surface Quality", in *83rd Steelmaking Conference Proceedings*, vol. 83, (Pittsburgh, PA, March 26-29, 2000), ISS, Warrendale, PA, 2000, pp. 461-76.

5. J. Knoepke and M. Hubbard: "Pencil Blister Reductions at Inland Steel Company", in *77th Steelmaking Conference Proceedings*, vol. 77, (Chicago, IL, March 20-23, 1994), ISS, Warrendale, PA, 1994, pp. 381-88.

6. I. Sasaka, T. Harada, H. Shikano and I. Tanaka: "Improvement of Porous Plug and Bubbling Upper Nozzle for Continuous Casting", in *74th ISS Steelmaking Conference*, vol. 74, (Washington, D.C., April 14-17, 1991), ISS, Warrendale, PA, 1991, pp. 349-56.

7. B.G. Thomas, A. Dennisov and H. Bai: "Behavior of Argon Bubbles during Continuous Casting of Steel", in *80th ISS Steelmaking Conference Proceedings*, vol. 80, (Chicago, IL, April 13-16, 1997), ISS, Warrendale, PA, 1997, pp. 375-84.

8. H. Buhr and J. Pirdzun: "Development of Refractories for Continuous Casting", *Continuous Casting of Steel*, (Biarritz, France), 1976.

9. E.S. Szekeres: "Review of Strand Casting Factors Affecting Steel Product Cleanliness", *4th International Conference on Clean Steel*, (Balatonszeplak, Hungary), 1992.

10. H.H. Ozeki, T. Yamaguchi, T. Takasu and T. Auki: "Prevention of Alumina Clogging in Tundish Shroud", *2nd International Conference on Refractories*, (Japan), Tech Association of Refractories, 1987, pp. 398-410.

11. N.A. McPherson and S.L. McIntosh: "Mould Power Related Defects in Some Continuously Casting Steel Products", in *70th Steelmaking Conference Proceedings*, vol. 70, ISS, Warrendale, PA, 1987, pp. 17-25.

12. W.H. Emling, T.A. Waugaman, S.L. Feldbauer and A.W. Cramb: "Subsurface Mold Slag Entrainment in Ultra-Low Carbon Steels", in *Steelmaking Conference Proceedings*, vol. 77, (Chicago, IL, April 13-16, 1997), ISS, Warrendale, PA, 1994, pp. 371-79.

13. S.M. Dawson: "Tundish Nozzle Blockage During the Continuous Casting of Aluminum-killed Steel", in *73rd Steelmaking Conference Proceedings*, vol. 73, (Detroit, MI, Mar 25-28, 1990), ISS, Warrendale, PA, 1990, pp. 15-31.

14. H.T. Tsai: *Water Modeling on Pressure Profile in the Tundish Shroud at Flo-Con*, ISPAT-Inland Steel, East Chicago, IN, Report, 1986.

15. L. Wang, H.-G. Lee and P. Hayes: "Modeling of air ingress and pressure distribution in ladle shroud system for continuous casting of steel", *Steel Research,* 1995, vol. 66 (7), pp. 279-86.

16. H. Bai and B.G. Thomas: "Turbulent Flow of Liquid Steel and Argon Bubbles in Slide-Gate Tundish Nozzles, Part I, Model Development and Validation", *Metall. Mater. Trans. B,* 2001,, p. in press.

17. H. Bai and B.G. Thomas: "Turbulent Flow of Liquid Steel and Argon Bubbles in Slide-Gate Tundish Nozzles, Part II, Effect of Operation Conditions and Nozzle Design", *Metall. Mater. Trans. B,* 2001,, p. in press.

18. U. Sjöström, M. Burty, A. Gaggioli and J. Radot: "An Experimental Study of Argon Injection and Aspiration of Air into Stopper Rod in Continuous Casters", in *81st Steelmaking Conference Proceedings*, vol. 81, (Toronto, Canada, March 22-25, 1998), ISS, Warrendale, PA, 1998, pp. 63-71.

19. *CFX 4.2 Users Manual*, AEA Technology, 1700 N. Highland Rd., Suite 400, Pittsburgh, PA 15241, program, 1998.

20. M.T. Heath: *Scientific Computing, An Introductory Survey*, McGraw-Hill, New York, 1997.

21. H. Bai: *Argon Bubble Behavior in Slide-Gate Nozzles during Continuous Casting of Steel Slabs*, Ph.D. Thesis, University of Illinois at Urbana-Champaign, 2000.

22. R. Gass: Inland Steel, private communication, 1998.

23. F.M. Najjar, B.G. Thomas and D. Hershey: "Numerical Study of Steady Turbulent Flow through Bifurcated Nozzles in Continuous Casting", *Metallurgical Transactions B,* 1995, vol. 26B (4), pp. 749-65.

24. Y.H. Wang: "3-D Mathematical Model Simulation on the Tundish Gate and Its Effect in the Continuous Casting Mold", in *10th Process Technology Conference Proc*., vol. 10, (Toronto, Canada, April 5-8, 1992), ISS, Warrendale, PA, 1992, pp. 271-78.

25. M.B. Assar: LTV Steel Research, Independence, OH, private communication, 1998.

26. B.G. Thomas, X. Huang and R.C. Sussman: "Simulation of Argon Gas Flow Effects in a Continuous Slab Caster", *Metallurgical Transactions B,* 1994, vol. 25B (4), pp. 527-47.

27. M. Burty, M. Larrecq, C. Pusse and Y. Zbaczyniak: "Experimental and Theoretical Analysis of Gas and Metal Flows in Submerged Entry Nozzles in Continuous Casting", in *13th PTD Conference Proceedings*, vol. 13, (Nashville, TN, April 2-5, 1995), ISS, Warrendale, PA, 1995, pp. 287-92.

28. H. Bai and B.G. Thomas: "Bubble Formation during Horizontal Gas Injection into Downward Flowing Liquid", *Metallurgical and Materials Transactions B,* 2001,, p. under review.

Table I. Nozzle dimensions and operating conditions

Dimension & Condition	Standard Nozzle	Validation Nozzle A	Validation Nozzle B
UTN top diameter (mm)	114	115	100
UTN length (mm)	241.5	260	310
Gate thickness(mm)	63	45	45
Gate diameter(mm)	78	75	70
Shroud holder thickness (mm)	100	100	66
SEN length (mm)	748	703	776
SEN bore diameter (mm)	78	91-96	80
SEN submerged depth (mm)	200	120-220	165
Port width X height (mm X mm)	78X78	75X75	78X78
Port thickness(mm)	29	30	28.5
Port angle (down)	15°	35°	15°
Recessed bottom well depth (mm)	12	12	12
Slide gate orientation	90°	90°	90°
Gate opening (F_L)	50%		52%
Casting speed (V_C) (m/min, 8”x52”slab)	1		1.21
Liquid flow rate (l/min)	268.4		324.8
Tundish depth (H_T) (m)		1.125	0.927
Argon injection flow rate (Q_G) (SLPM)	10	7-10	14
Argon injection (hot) volume fraction f_g	16%		17.7%
Argon bubble diameter (D) (mm)	1	1	1

Table II Simulation conditions for the standard nozzle

Variable	Value	Notes
Casting Speed V_C (m/min)	0.2, 0.5, 1, 1.5, 2.0, 2.3	For 8"x52" slab
Gate Opening F_L (%)	40, 50, 60, 70, 100	Linear opening
Argon Flow Rate Q_G (SPLM)	0, 5, 10	"cold" argon
Nozzle Bore Diameter D_B (mm)	60, 70, 78, 90	Also simulates clogging

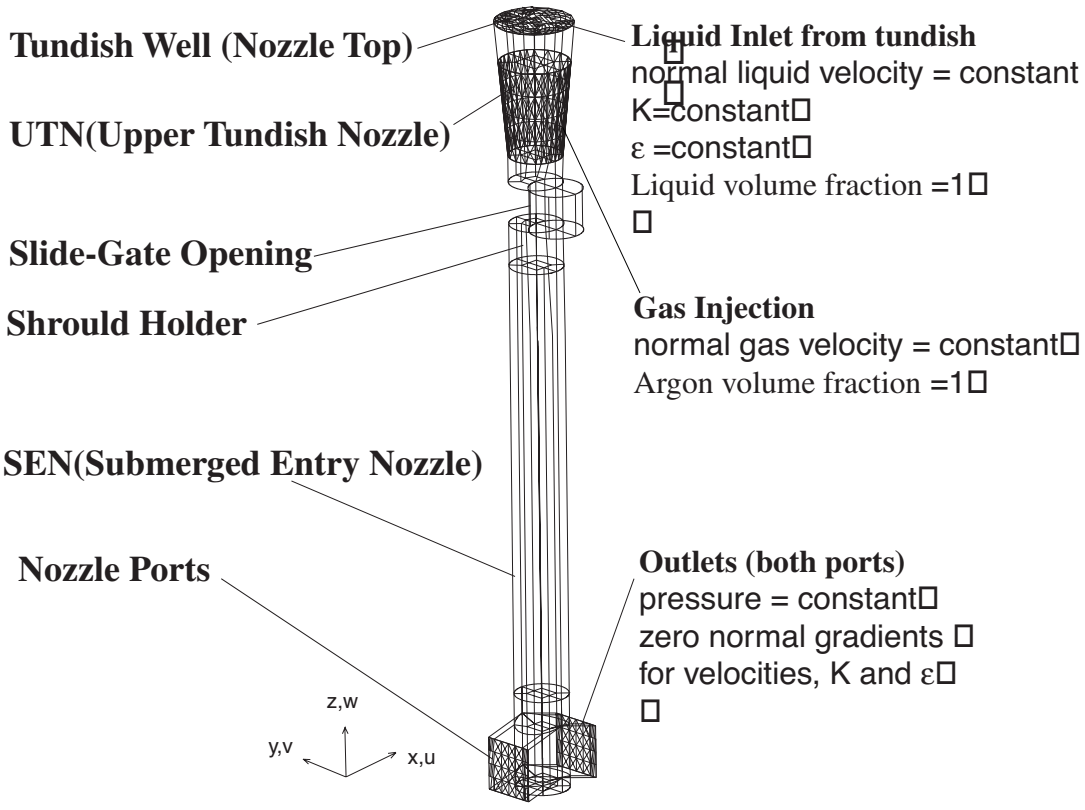

Figure 1. Computational domain and boundary conditions for the standard nozzle

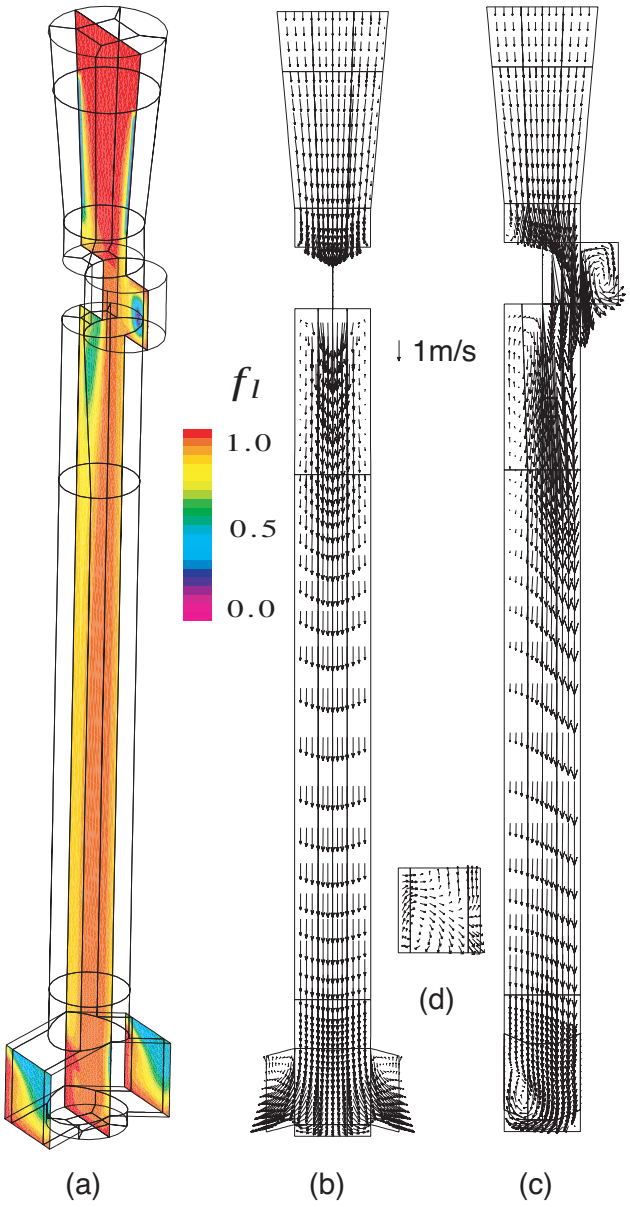

Figure 2. Simulated flow field for the standard nozzle and conditions in Table I
(a) Argon gas distribution (b) Velocities in center plane parallel to WF
(c) Velocities in center plane parallel to NF (d) Velocities at port outlet plane

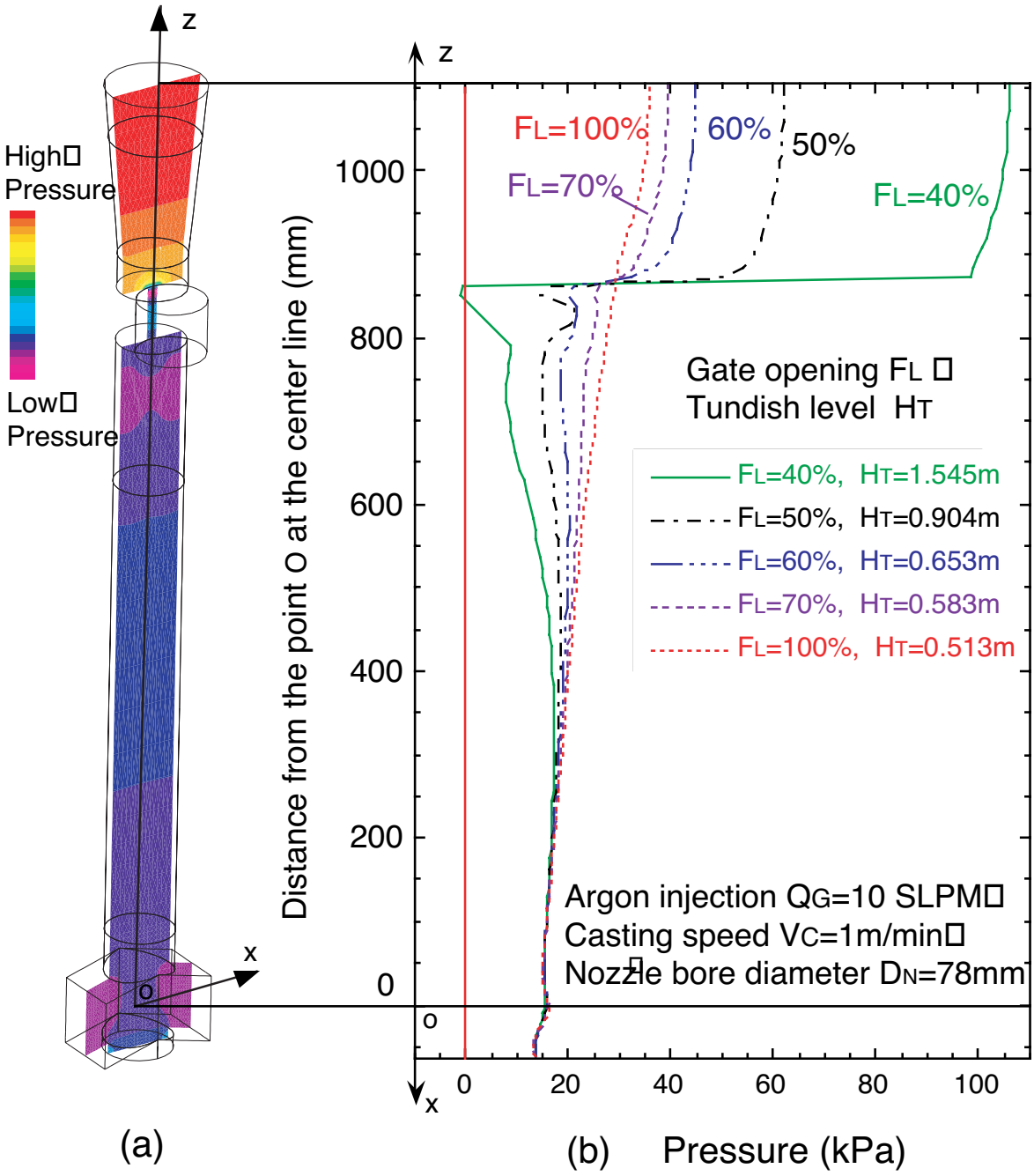

Figure 3. Pressure distribution in the standard nozzle, predicted by the 3-D finite difference model (a) shaded contour plot at the center-plane (b) pressure profile along the centerline (from top to outlet port)

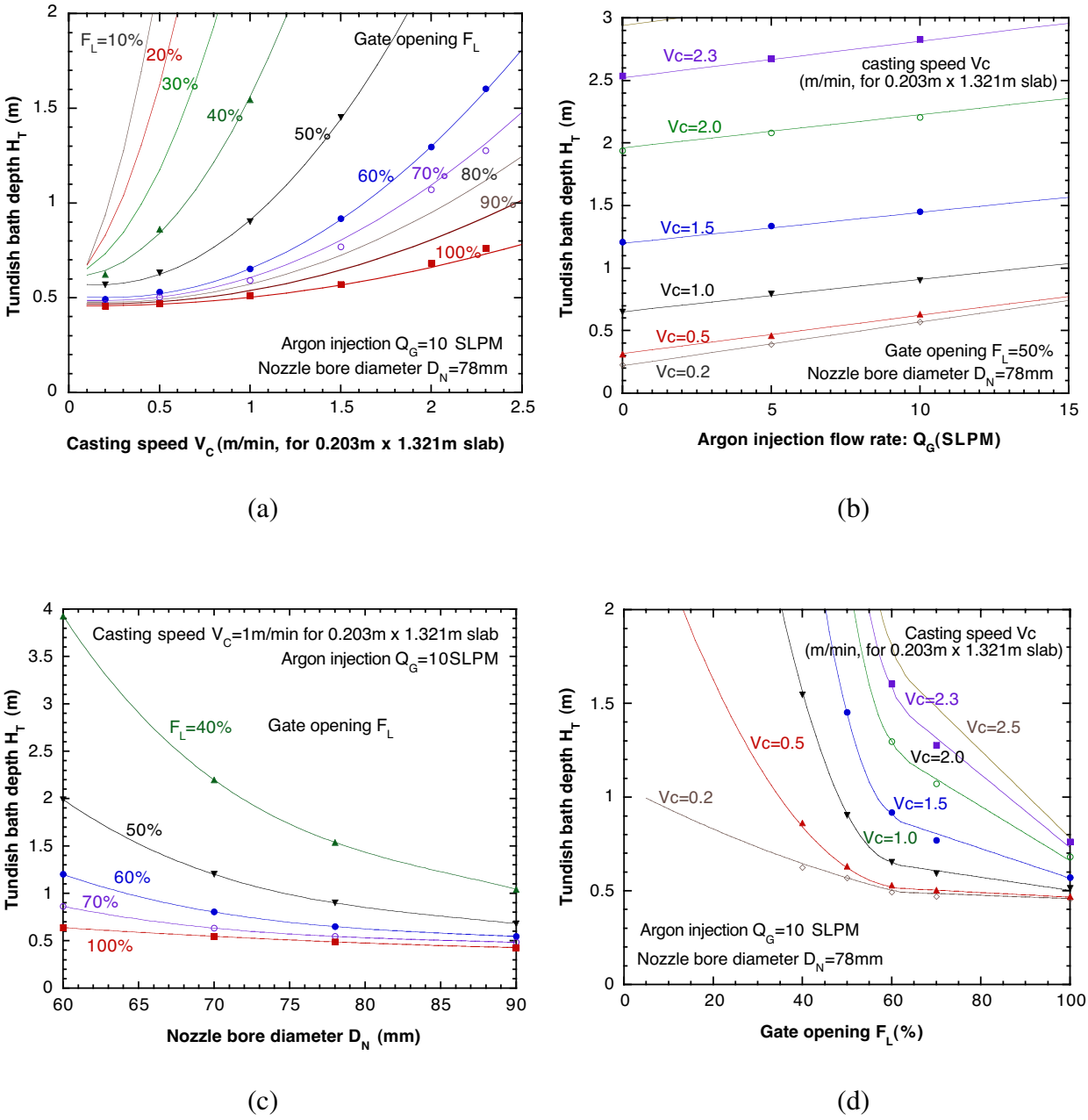

Figure 4 CFX model output (points from Equation 1) and fitting curve (lines of Equation A2) showing effects of casting speed, gate opening, argon injection and nozzle bore size

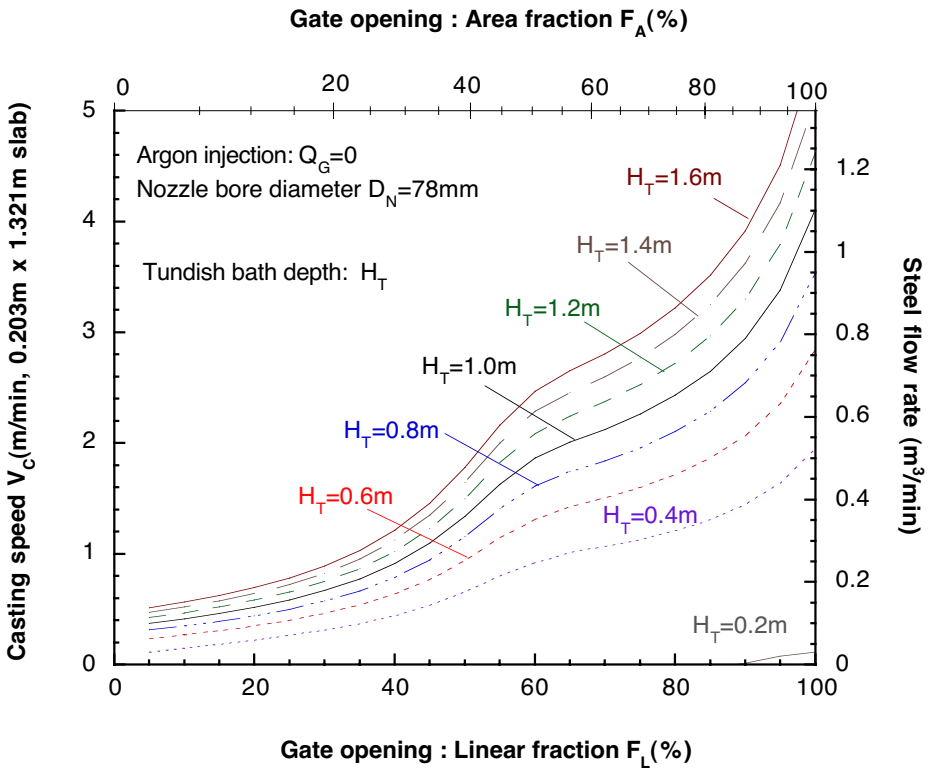

(a)

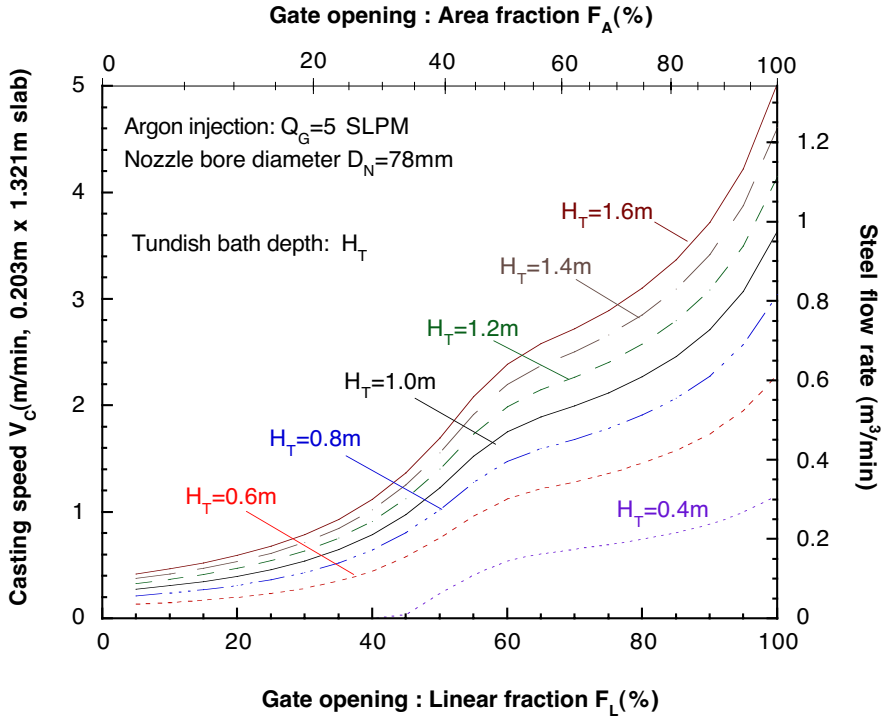

(b)

Figure 5 Inverse model plots showing effect of gate opening and tundish bath depth on casting speed (a) No gas injection (b) 5 SLPM argon injection

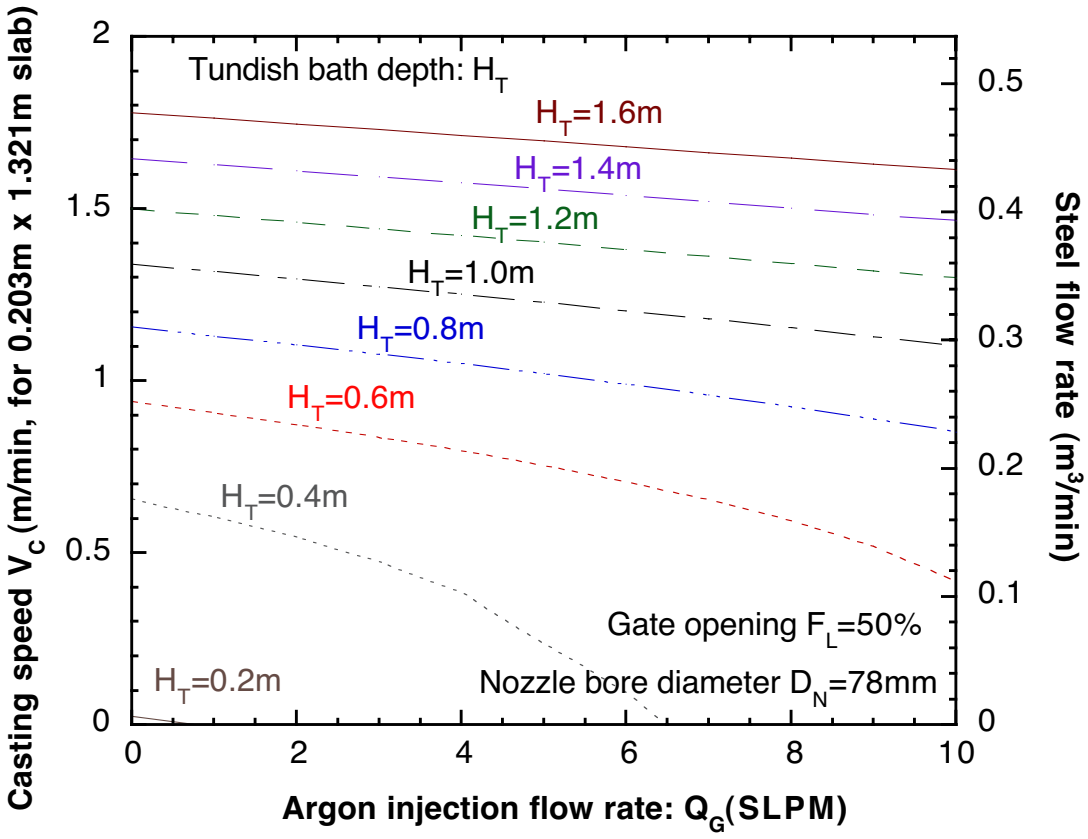

Figure 6. Inverse model plots showing effect of gas injection and tundish bath depth on casting speed

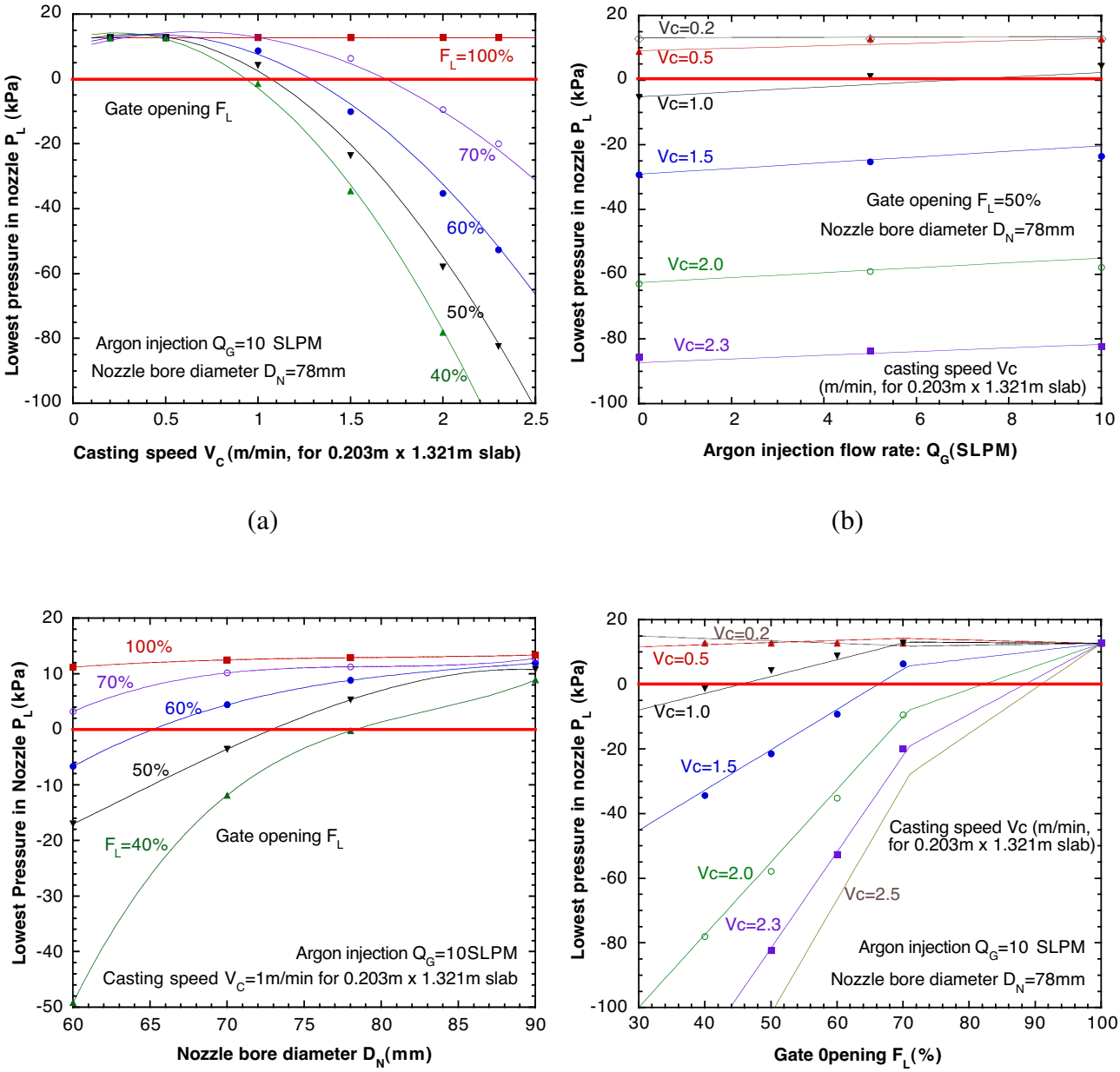

Figure 7. CFX model output (points) and fitting curve (lines of Equations 2) showing effects of casting speed, gate opening, argon injection and nozzle bore size on the lowest pressure P_L in nozzle (under varying tundish bath depth)

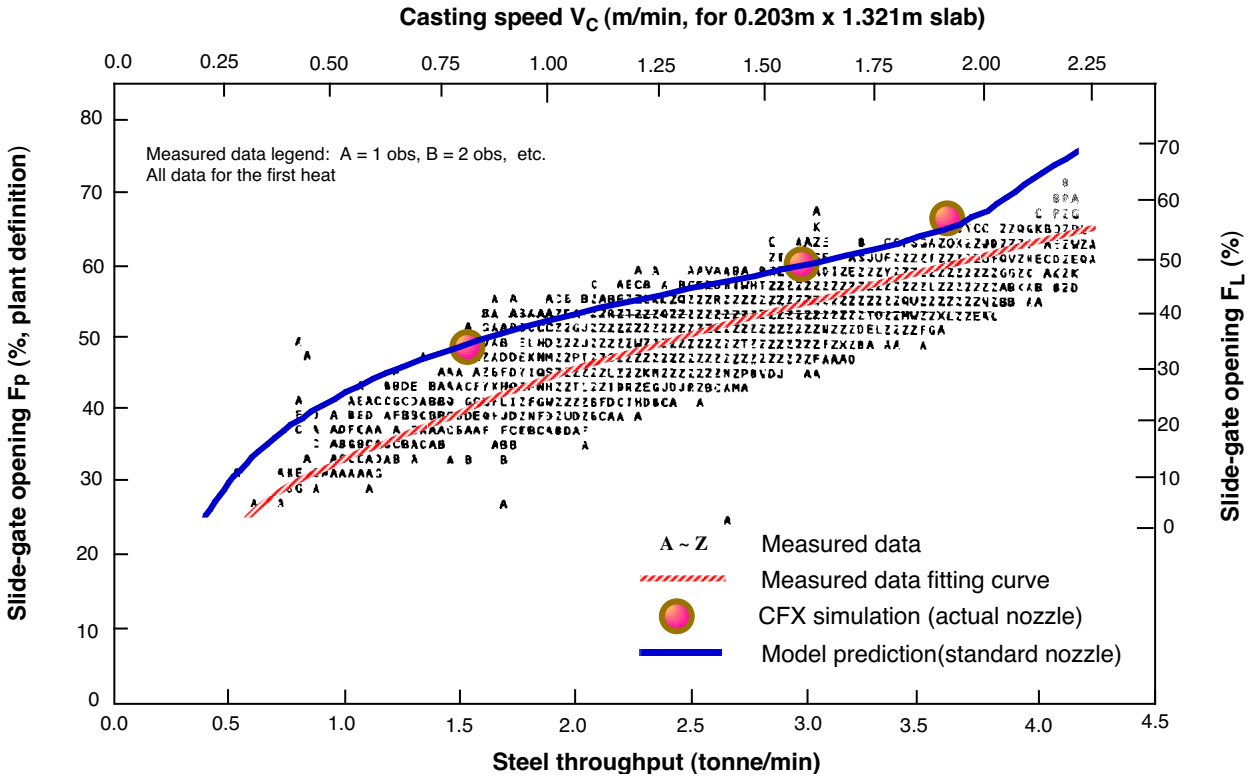

Figure 8. Comparison of measured and model predicted relationship between opening restriction fraction and steel flow rate

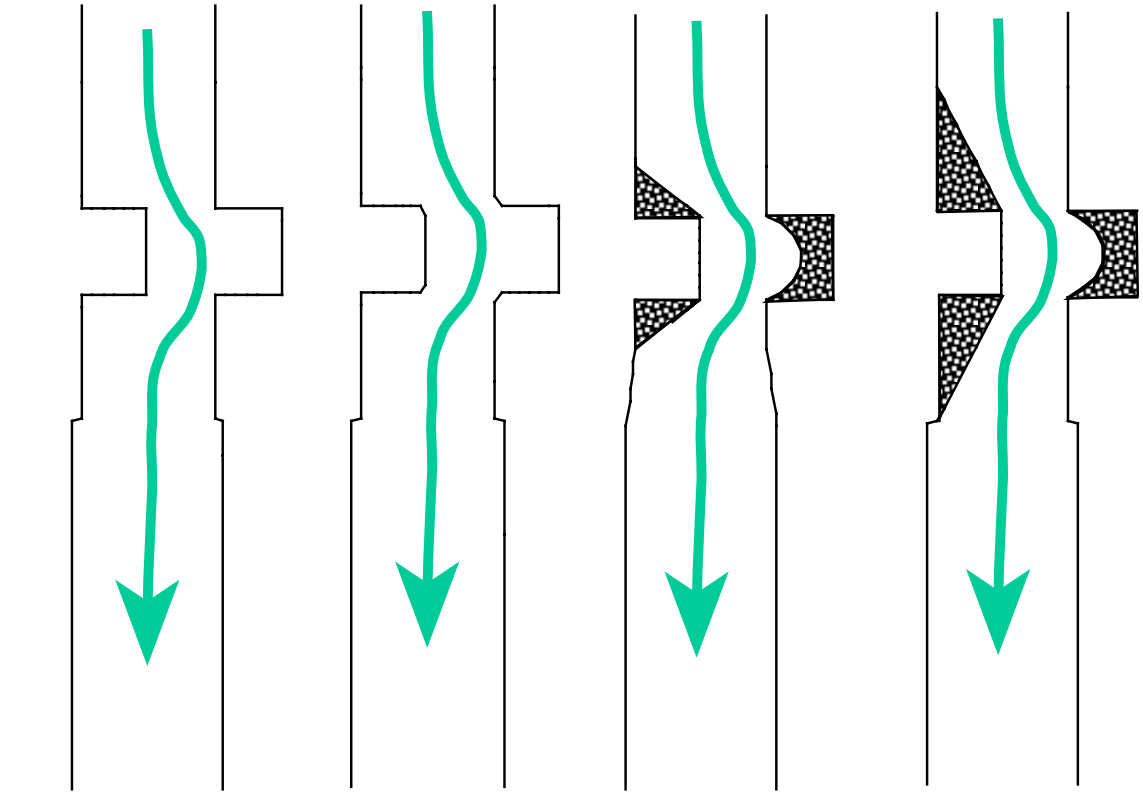

Figure 9. Assumed shape of initial clogging and rounded edges in the vicinity of the slide-gate (Validation Nozzle B)

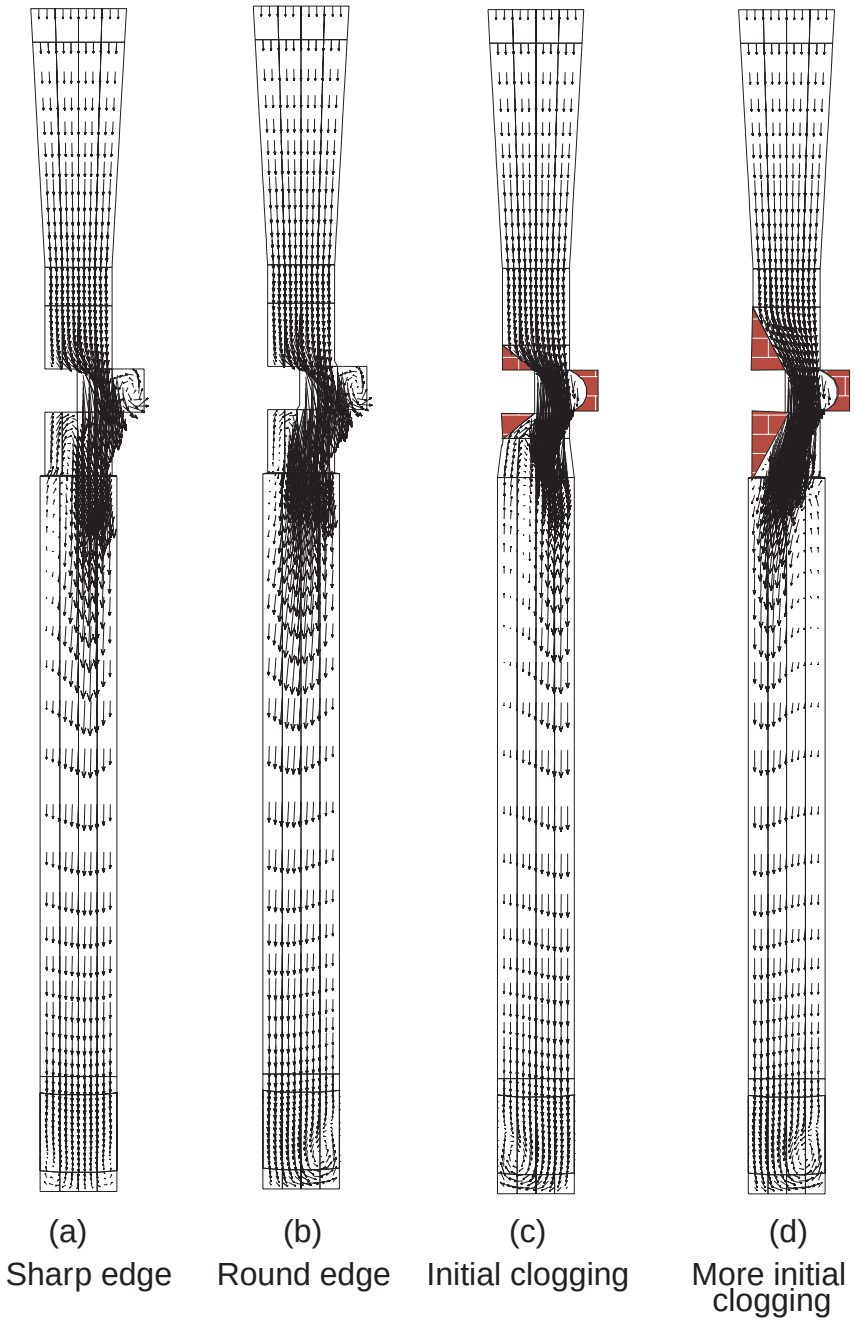

Figure 10. Effects of initial clogging and rounded edges on nozzle flow pattern (center plane parallel to the narrow face for Validation Nozzle B)

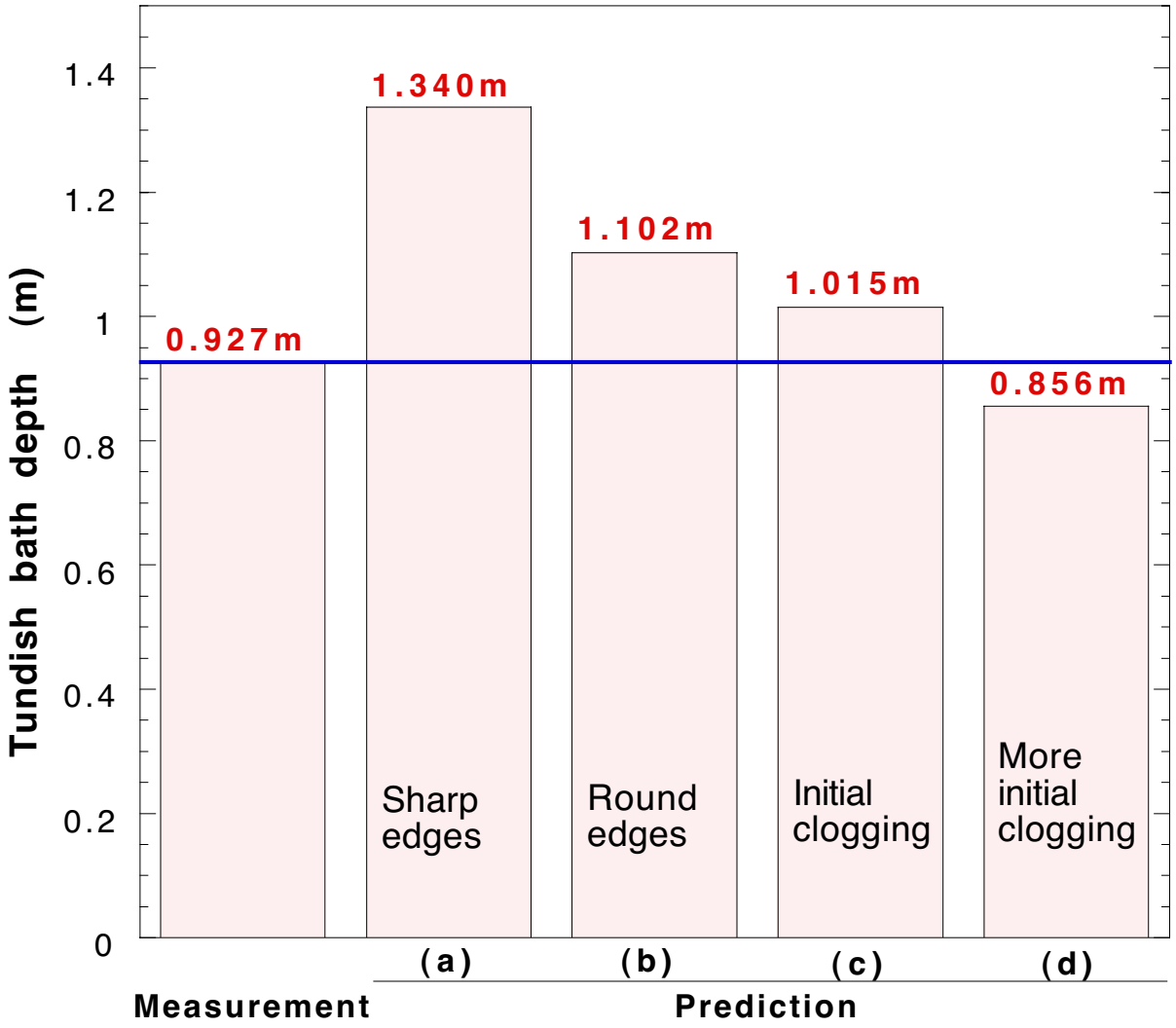

Figure 11. Effects of initial clogging and rounded edges on predicted tundish bath depth (Validation Nozzle B)

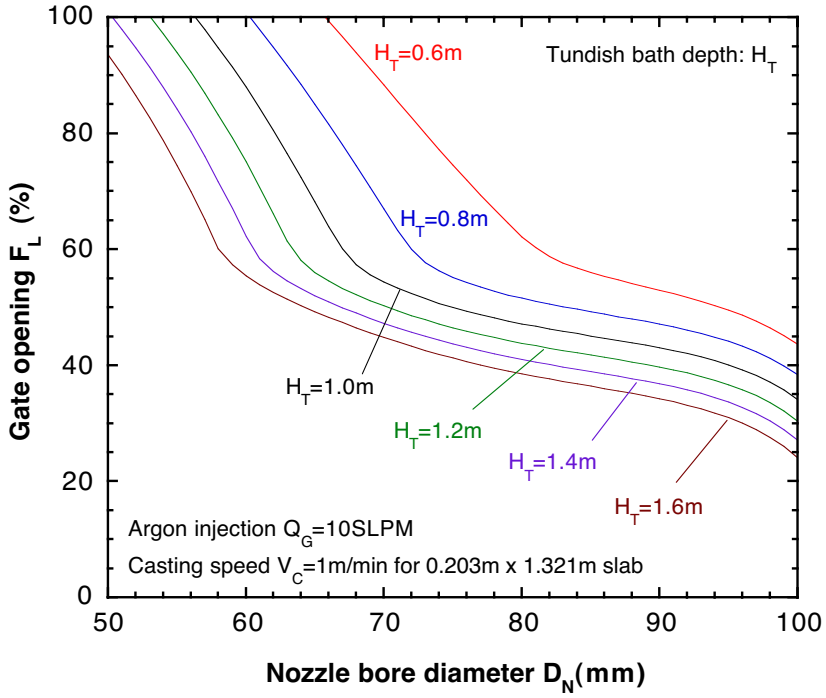

(a) Gate opening changes required for fixed casting speed

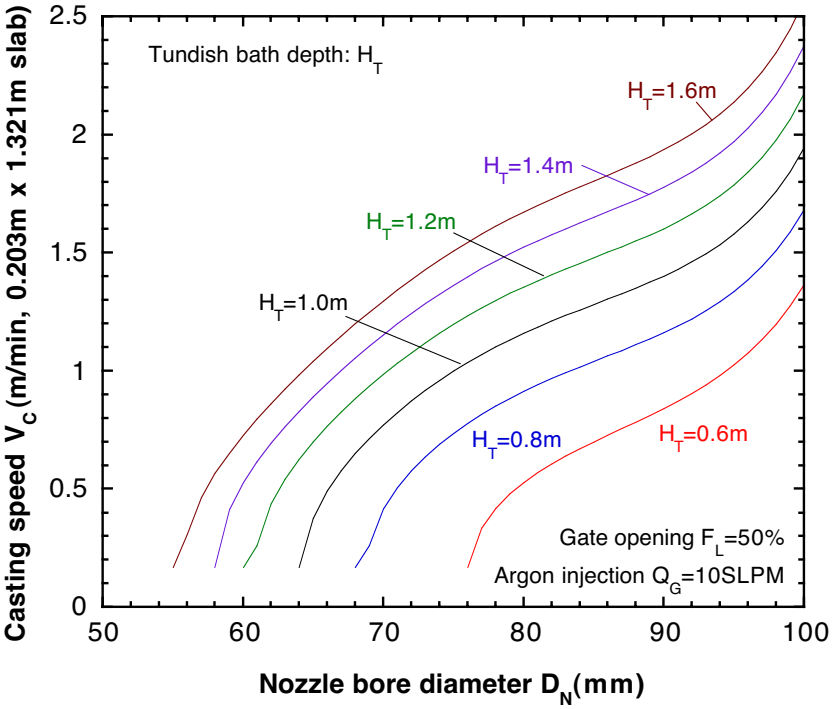

(b) Casting speed changes caused at fixed gate opening

Figure 12. Effects of change in nozzle bore size (such as caused by clogging)

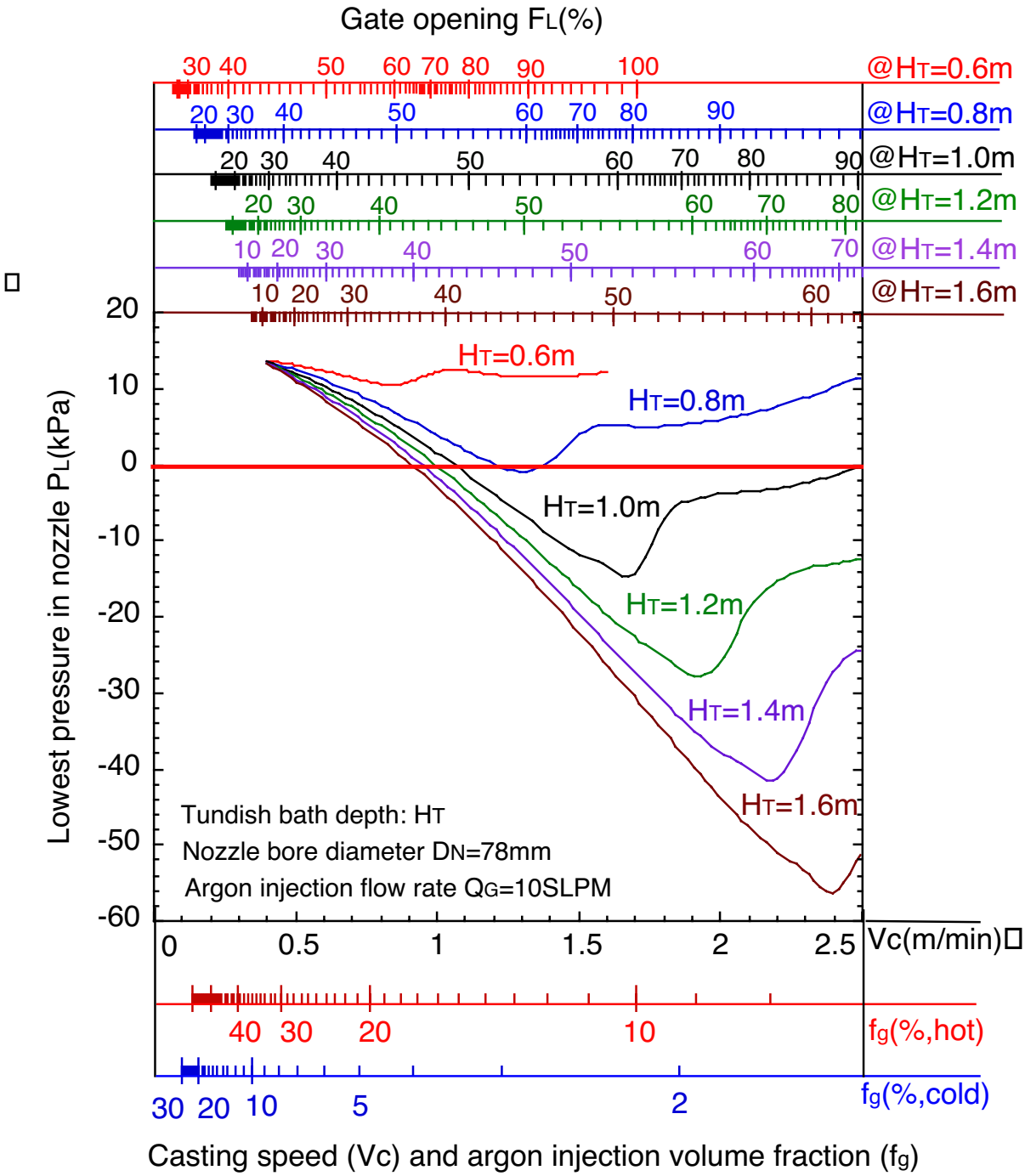

Figure 13 Effect of casting speed on minimum pressure in the nozzle for constant tundish bath depth and argon injection flow rate
(a) 10 SLPM argon injection, 78 mm nozzle bore

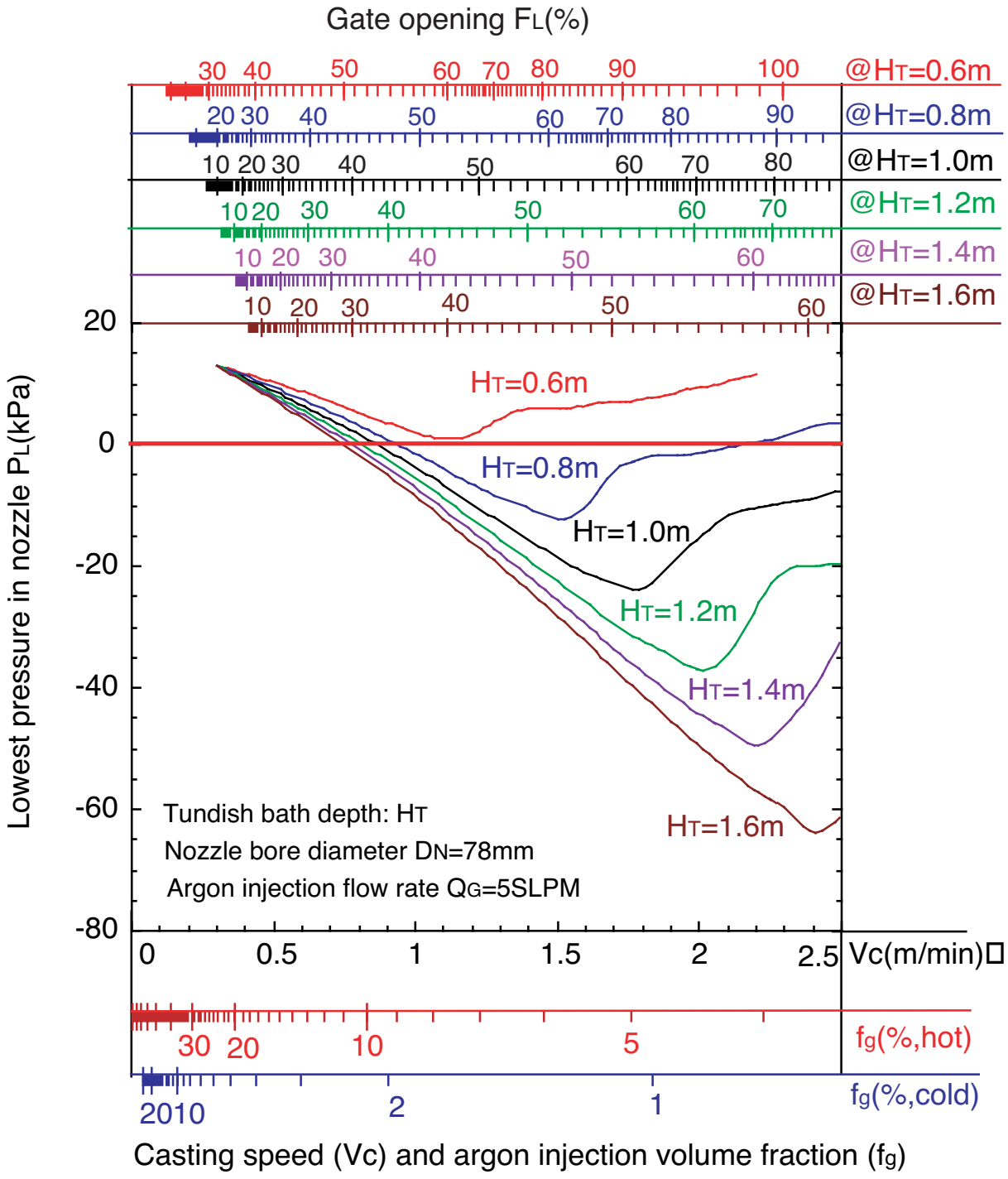

Figure 13 Effect of casting speed on minimum pressure in the nozzle for constant tundish bath depth and argon injection flow rate
(b) 5 SLPM argon injection, 78 mm nozzle bore

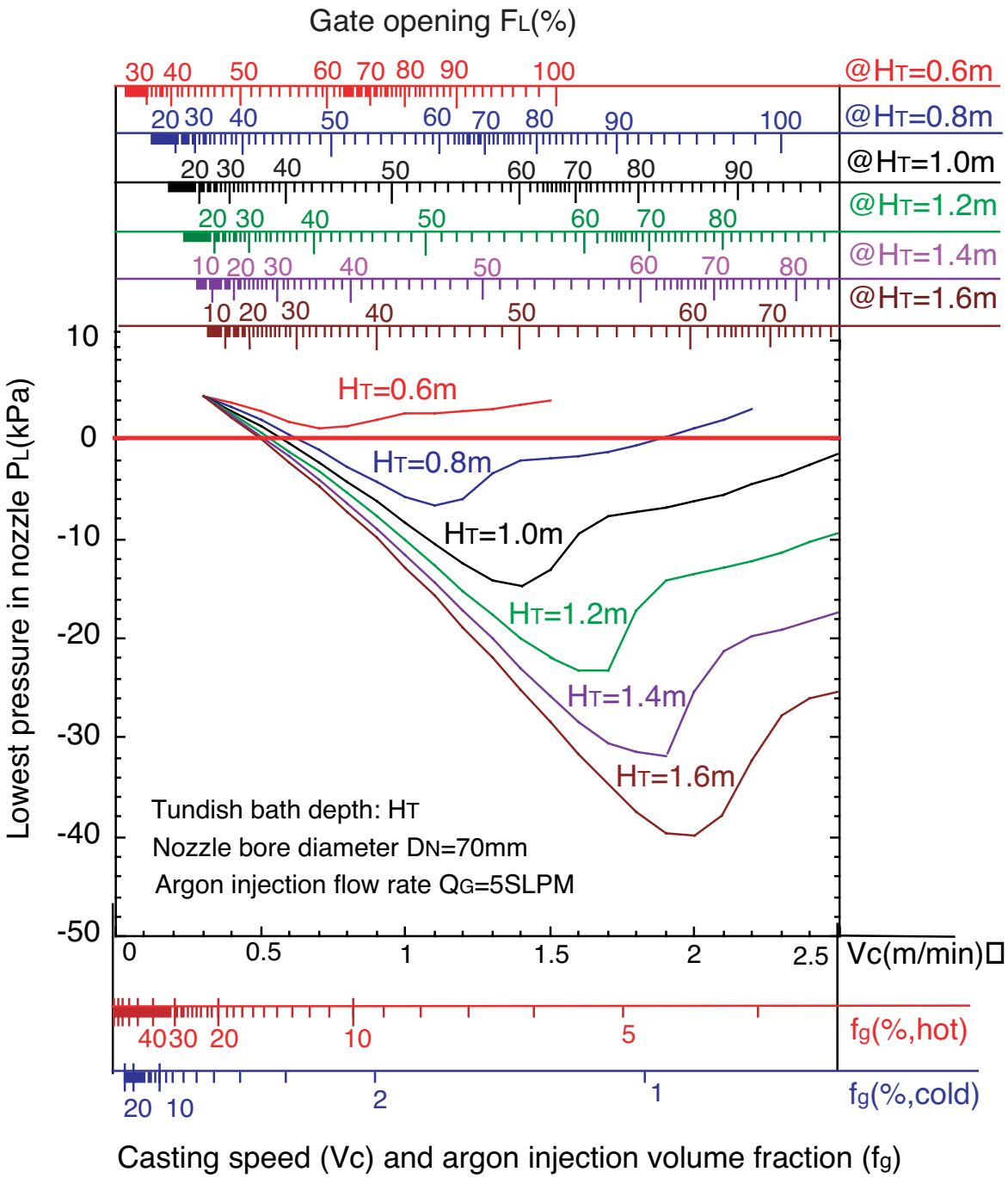

Figure 13 Effect of casting speed on minimum pressure in the nozzle for constant tundish bath depth and argon injection flow rate
(c) 5 SLPM argon injection, 70 mm nozzle bore

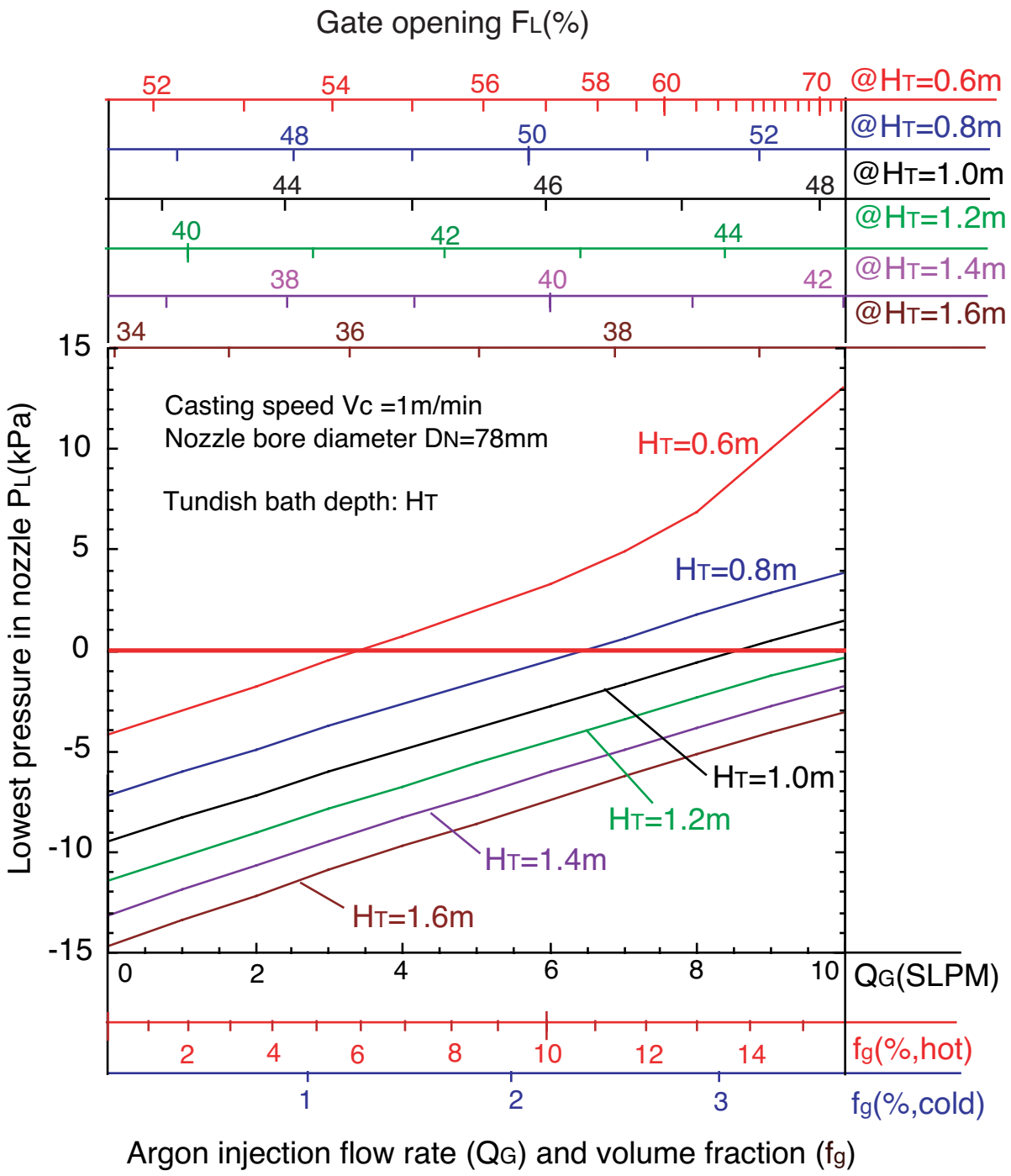

Figure 14 Effect of argon injection flow rate on minimum pressure in the nozzle for constant tundish bath depth and casting speed
(a) 1 m/min casting speed, 78 mm nozzle bore

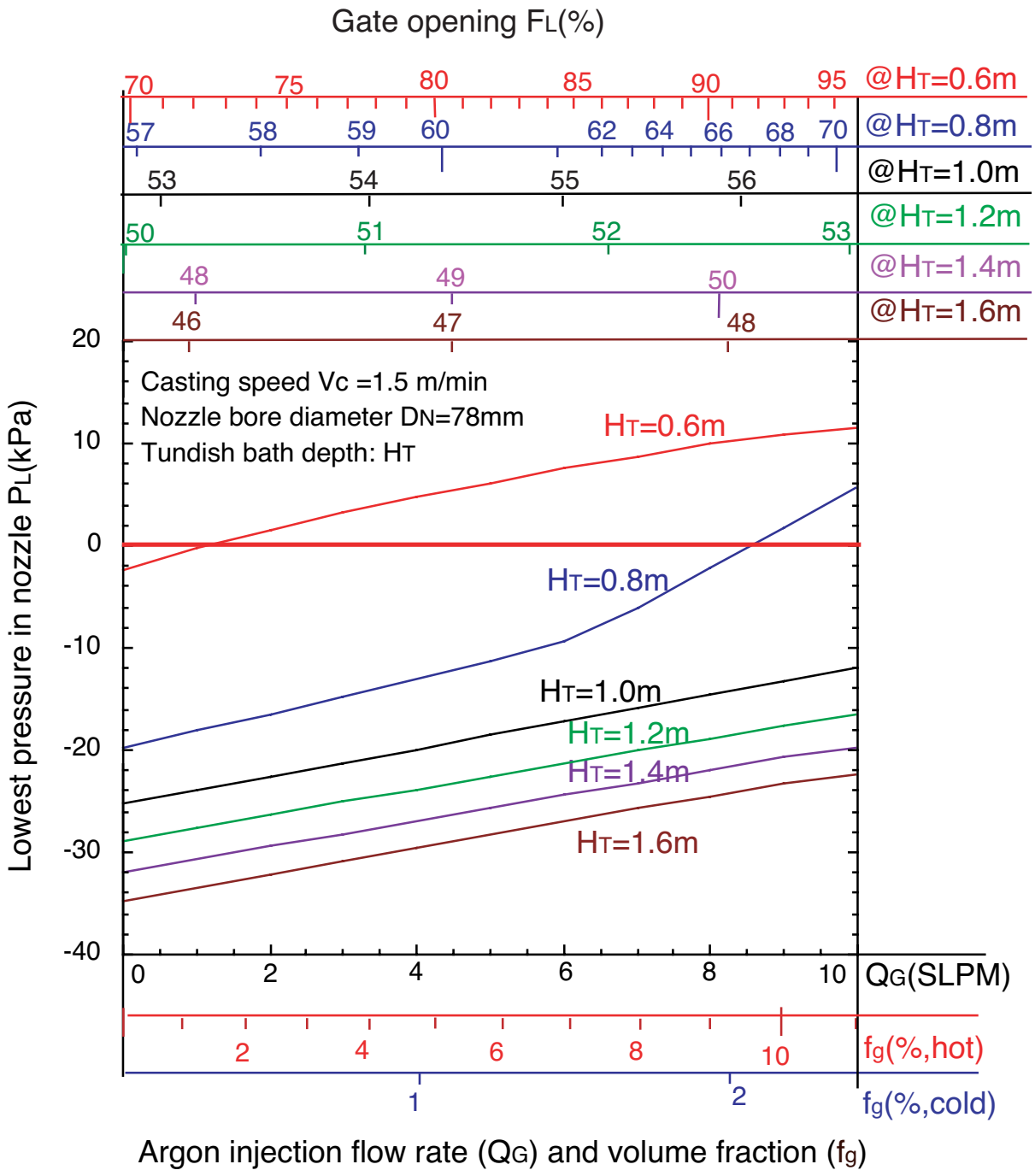

Figure 14 Effect of argon injection flow rate on minimum pressure in the nozzle for constant tundish bath depth and casting speed
(b) 1.5 m/min casting speed, 78 mm nozzle bore

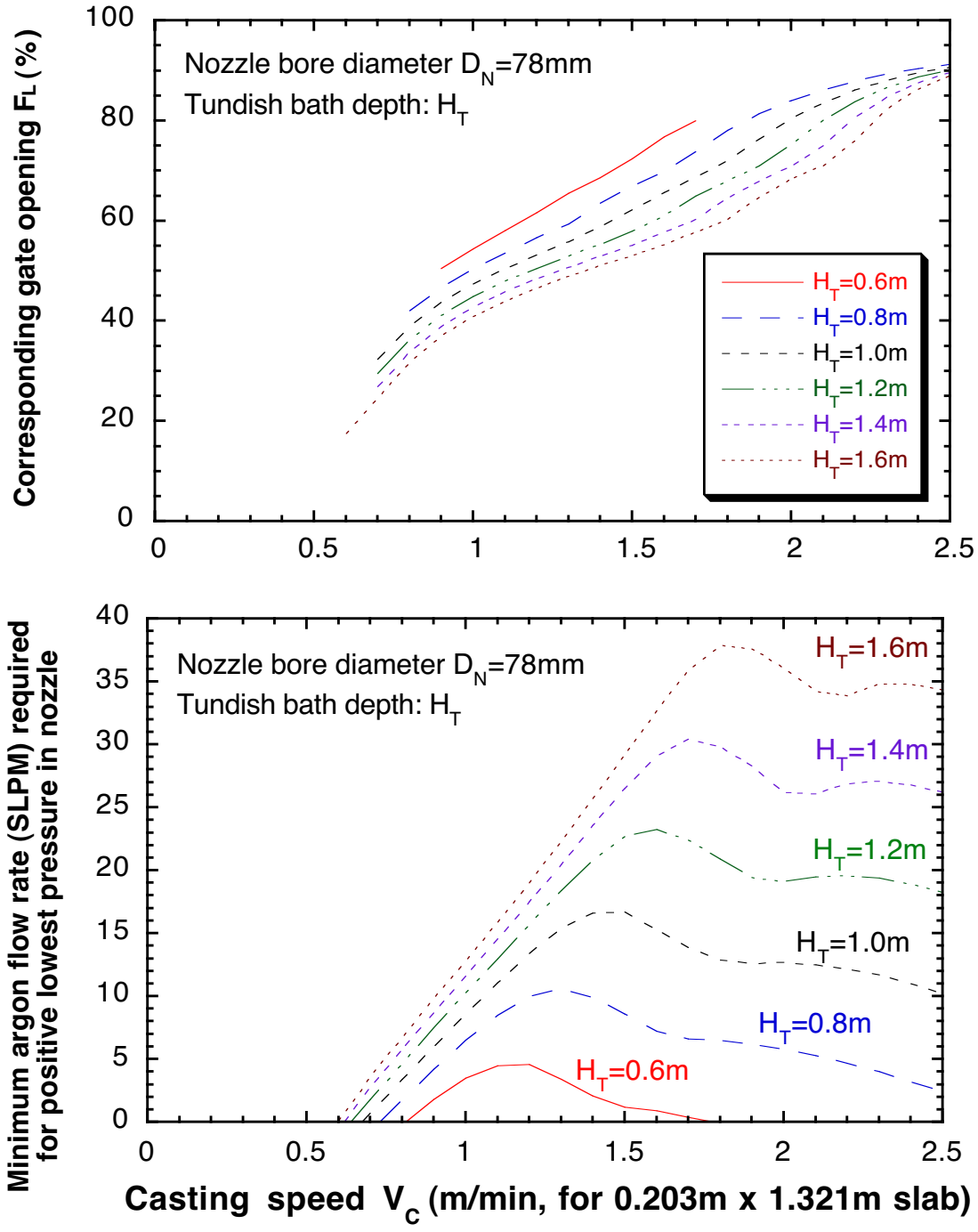

Figure 15. Effect of casting speed and tundish depth on minimum argon flow rate required for positive pressure in nozzle (bottom) and the corresponding gate opening (top)
(a) 78 mm nozzle bore

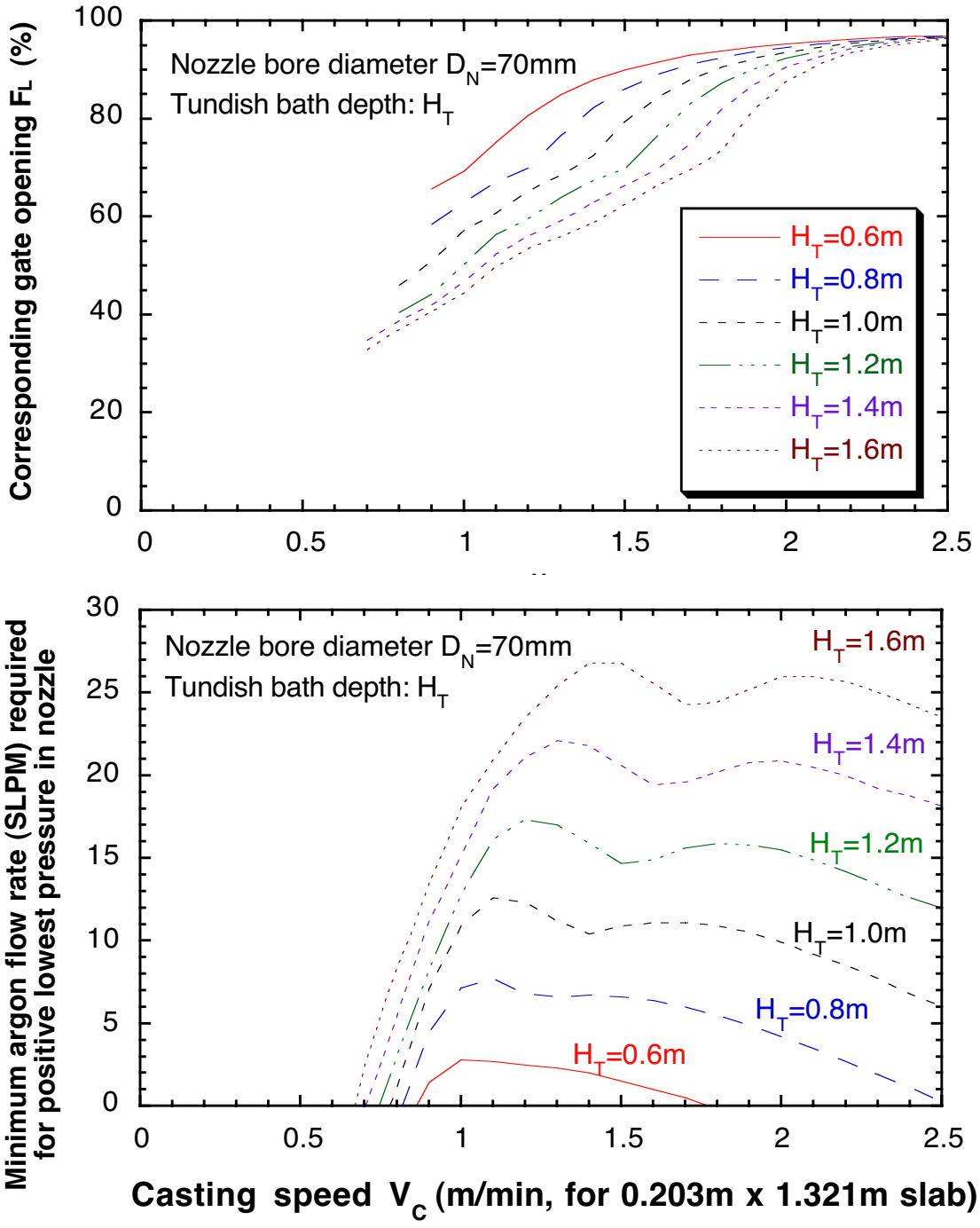

Figure 15. Effect of casting speed and tundish depth on minimum argon flow rate required for positive pressure in nozzle (bottom) and the corresponding gate opening (top)
(b) 70 mm nozzle bore